Generalized Passive Radar Processing Chain For Use With Different Signals of Opportunity

Prepared by:
Heinrich Stephen Benz

Prepared for:
Dr Stephen Paine
Department of Electrical Engineering
University of Cape Town

Submitted to the Department of Electrical Engineering at the University of Cape Town
in partial fulfilment of the academic requirements for a
Masters of Science in Engineering specialising in Radar and Electronic Defence

November 28, 2023

Declaration

1. I know that plagiarism is wrong. Plagiarism is to use another's work and pretend that it is one's own.
2. I have used the IEEE convention for citation and referencing. Each contribution to, and quotation in, this report from the work(s) of other people has been attributed, and has been cited and referenced.
3. This report is my own work.
4. I have not allowed, and will not allow, anyone to copy my work with the intention of passing it off as their own work or part thereof.

Signed by candidate

November 28, 2023

Heinrich Benz

Date

Acknowledgements

I would like to extend my thanks to Dr. Stephen Paine, my supervisor, for patiently teaching me and aiding me through this Masters. I am also extremely grateful for the opportunities he provided to expand my horizons in the field, both academically and otherwise.

I would like to thank my professors for introducing me to fascinating topics and knowledge. Specifically, Dr Francois Maasdorp and Christo Cloete for their fascinating and insightful course on Electronic Defense.

I would like to thank my peers in the Radar Remote Sensing Group (RRSG) at UCT for their good humour and valuable insights. Among others, I wish Grant Norrie, Thomas Gwasira and Tlotliso Mapana all the best.

To those that I have worked with throughout this couple of years, both directly connected to my masters and indirectly. Jan Pidanic, Prof. Amit Mishra, Christof Schüpbach.

To my grandparents Hein and Linnie, without whom this postgraduate would have been next to impossible for me. Your support and love is invaluable to me and I am forever grateful for all that have and still do for me.

Lastly, I would like to thank my parents, Rina and Alfred, for supporting my endeavors with so much love. Thank you for always being there for me, I could not have made it this far without you.

Abstract

A Passive Radar (PR) is a multi-static RAdio Detection and Ranging (radar) that makes use of signals transmitted by Illuminators of Opportunity (IoO)'s to detect targets in a scene. An IoO is any preexisting transmitter that is used as the illuminator for the PR such as Frequency Modulation (FM) radio. The exact performance of a PR depends on both the physical geometry of the transmitter and receiver combination as well as the signal properties of the IoO.

By using multiple different IoO's concurrently, transmitter diversity can be increased, improving overall system performance and reliability as well as improving resilience against jamming. Typically this would require separate processing pipelines specific to each signal type. This is cumbersome, requiring separate maintenance, deployment and streamlining for each one. In this project a generalised PR processing pipeline capable of efficiently processing any signal to create an appropriate range-Doppler output is proposed and demonstrated.

A typical PR processing pipeline consists of primarily four stages; pre-processing, DSI-cancellation, range-Doppler map generation and finally detection and tracking. The pre-processing stage is signal dependant and therefore cannot be generalized. DSI-cancellation is the most resource intensive of the stages and along with range-Doppler map generation, detection and tracking can be generalised.

Digital signals such as Orthogonal Frequency Division and Multiplexing (OFDM) signals have high bandwidths and are required to be processed in the Frequency-Domain (FD). Therefore, an appropriate FD Direct Signal Interference (DSI) cancellation algorithm that works for both analogue and digital signals was necessary for the generalised processing pipeline. For this, an investigation into the use of Extensive Cancellation Algorithm by Carrier/Doppler (ECA-CD), a FD approach, applied to FM signals for generalisation was carried out. By generating Amplitude Range-Doppler (ARD) maps and comparing the results to ARD maps generated when using Conjugate Gradient Least Square (CGLS), a Time Domain (TD) approach, for cancellation, it was found that ECA-CD is an effective and efficient cancellation algorithm for FM signals. It was, therefore, selected as the DSI-cancellation algorithm for the processing chain.

To demonstrate the feasability of the suggested chain, three signals were used; FM, DVB-T2 and Long Term Evolution (LTE) as these represent some of the most commonly used IoO's. The results demonstrate that an efficient generalised processing chain can be realised using an FD approach with ECA-CD for DSI-cancellation and Batches for ARD processing.

Contents

List of Figures

Abbreviations

AAF Auto Ambiguity Function

ADC Analogue-to-Digital Converters

AF Ambiguity Function

AM Amplitude Modulation

AR Active Radar

ARD Ambiguity Range Doppler

BBC British Broadcasting Corporation

BPSK Binary Phase Shift Keying

CAF Cross Ambiguity Function

CFAR Constant False Alarm Rate

CGLS Conjugate Gradient Least Square

CP Continual Pilots

CPI Coherent Processing Interval

CR Commensal Radar

DAB Digital Audio Broadcasting

DFT Digital Fourier Transform

DSI Direct Signal Interference

DVB Digital Video Broadcasting

DVB-T Digital Video Broadcasting – Terrestrial

DVB-T2 Digital Video Broadcasting — Second Generation Terrestrial

EAN European Aviation Network

ECA Extensive Cancellation Algorithm

ECA-C Extensive Cancellation Algorithm by Carrier

ECA-CD Extensive Cancellation Algorithm by Carrier/Doppler

EM Electromagnetic

FBLMS Frequency Domain Block Least Mean Square

FD Frequency Domain

FFT Fast Fourier Transform

FM Frequency Modulation

FX Fourier transform - Cross multiply

GP-GPUs General Purpose Graphics Processing Units

GSM Global System for Mobile communication

IFFT Inverse Fast Fourier Transform

IoO Illuminators of Opportunity

ISI Inter-Signal Interference

L1 Layer-1

LoS Line of Sight

LTE Long Term Evolution

LTE-R Long Term Evolution-Railway

MISO Multiple Input Single Output

OFDM Orthogonal Frequency-Division Multiplexing

PBR Passive Bistatic Radar

PCL Passive Coherent Location

PLP Physical Layer Pipes

PR Passive Radar

PSS Primary Synchronisation Symbol

QAM Quadrature Amplitude Modulation

radar RAdio Detection and Ranging

RB Resource Block

RCS Radar Cross-Section

RDS Radio Data System

RE Resource Element

RS Reference Signal

SAR Synthetic Aperture Radar

SDR Software Defined Radio

SISO Single Input Single Output

SKA Square Kilometer Array

SNR Signal to Noise Ratio

SP Scattered Pilots

SS Synchronisation Symbol

SSS Secondary Synchronisation Symbol

SVD Singular Value Decomposition

TD Time Domain

TV Television

UCT University of Cape Town

VCO Voltage Controlled Oscillator

WWII World War II

XF Cross multiply - Fourier transform

Chapter 1

Introduction

According to the standard definition in IEE686 RAdio Detection and Ranging (radar) is "an electromagnetic system for the detection and location of objects that operates by transmitting electromagnetic signals, receiving echoes from objects (targets) within its volume of coverage, and extracting location and other information from the echo signal. Note that (1) radar is an acronym for radio detection and ranging; (2) radar equipment can be operated with the transmitter turned off, as a passive direction finder on sources radiating within the band of the receiving system" [2]. There are applications for radar in many sectors, including mining, military, aviation, astronomy and more. Some common applications of radar include target detection, ranging, measuring position and velocity, determining the angle of arrival of a target echo and navigation.

There are two categories of Electromagnetic (EM) sensors [3], these being active and receive only. Active sensors have a dedicated transmitter, also known as an illuminator, that radiates the EM signal used in the radar. The receive only category is the relevant category for this work and includes passive sensors such as receive only signal analysers, direction finders and radio telescopes. The focus of this dissertation is the sub-category of passive sensors known as Passive Radar (PR).

PR's are radar systems that do not have a dedicated transmitter. Instead, they make use of existing transmitter infrastructure, typically in the form of commercial broadcast stations. An existing transmitter is referred to as an Illuminators of Opportunity (IoO). An IoO is a transmitter that the operator of the radar system has no control over. This includes both the transmitter location and the waveform being transmitted. There are various terms used to refer to PR systems, including Commensal Radar (CR), Passive Bistatic Radar (PBR) and Passive Coherent Location (PCL)[4, 5, 6]. This work will use the term PR as it is widely understood.

1.1 Overview of Passive Radar

PR has existed for as long as radar has existed, however, it has not seen wide use due to the challenges in its implementation when compared to traditional Active Radar (AR) systems. As technology has improved, more research into PR has been performed, increasing the viability of implementing PR in radar applications.

When compared to AR systems, PR systems are computationally expensive and have reduced performance due to an unknown and uncontrolled reference signal not designed for use in radar, significant clutter present in the received signals, dynamic range issues as a result of the zero-Doppler reference

signal and signal reconstruction in the case of digital systems.

By overcoming these drawbacks of PR systems, technology has allowed the advantages that PR has over AR to be exploited more readily. Specifically, improvements in digital processing hardware and the development of effective and efficient processing algorithms has made it viable to design PR systems with real-time processing in mind [4].

This leads to certain design considerations when selecting an IoO for PR use as not all IoO's will be suitable for a given application. The main considerations for an IoO to be considered suitable are the following [3, 7]:

- "The transmit power and antenna beam pattern must be suffcient for the desired coverage."
- "The modulation bandwidth of the illuminating signal should be suffcient to meet the desired range and Doppler resolutions."
- "Appropriate line of sight between potential transmitter-target and target-receiver pairs."

AR systems can be both monostatic and bistatic in nature, whereas PR systems are inherently bistatic. A monostatic radar has the transmitter and receiver co-located. The monostatic configuration results in a baseline of zero between the receivers, simplifying the necessary calculations for radar functions. Bistatic radar's on the other hand have the transmitter and receiver in seperate locations.

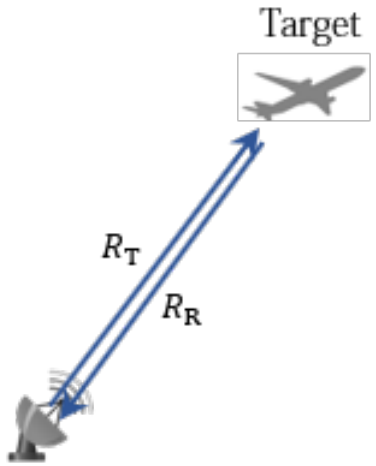

(a) Monostatic

Figure 1.1: Geometry of a monostatic radar where the transmitter and receiver are co-located.

Figure 1.1 illustrates the monostatic radar geometry. The transmitter and receiver are co-located. A defined signal is transmitted and the echoes are received in the same physical location.

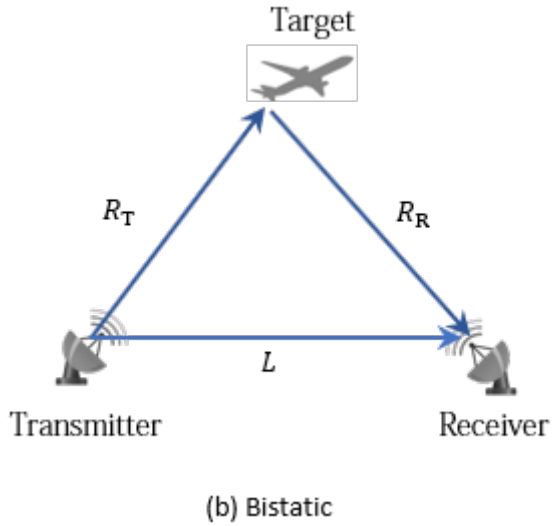

Figure 1.2: Geometry of a bistatic radar where the transmitter and receiver are in different locations.

The bistatic geometry in Figure 1.2 illustrates the separated transmitter and receiver architecture. PR systems are inherently bistatic as the transmitter cannot be a part of the designed radar. This geometry makes the necessary calculations more complex. The baseline L causes the reflection to occur at an angle known as the bistatic angle. The scattering paths R_T and R_R are rarely the same length will have different clutter profiles and propogation factors. These complicate performance modeling. The architecture also results in the possible target positions for each transmitter and receiver pair being elliptical, with foci at the transmitter and the receiver, rather than circular as would be expected in the monostatic case. However, this configuration does allow for advantageous placement of the antennae. It is also possible to increase the number of receivers and/or transmitters in different combinations to make what is known as a multi-static geometry. This may be useful for different applications, for example using multiple receivers to increase coverage or reduce the effect of obstacles and terrain. The overlapping range circles can also be used for positioning.

PR systems consist of an IoO, reference receiver and surveillance receiver. The reference channel is used to monitor the IoO waveform for the purpose of identifying echoes in the surveillance channel. The surveillance channel is used to detect echoes in the volume it monitors. This setup results in what is know as the Direct Signal Interference (DSI) in the surveillance channel. The DSI is the transmitted signal from the IoO received in the surveillance channel. Due to the echoes of the targets being orders of magnitude lower in power, the DSI masks targets and prevents target detection. The multipath effect adds to this problem as further reflections of the signal off of large static objects or terrain are received in the surveillance channel.

1.1.1 Co-located receivers

A PR with co-located receivers is beneficial for the processing of the channels as the distance between the two does not have to be accounted for. However, this does result in a strong DSI in the surveillance channel as illustrated in Figure 1.3. DSI and zero Doppler clutter removal is required to suppress the DSI in the surveillance channel to prevent the targets being masked. Zero Doppler clutter being the

delayed echoes of static objects.

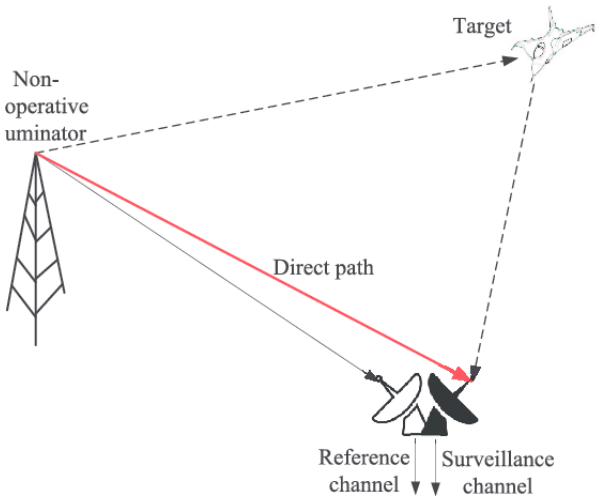

Figure 1.3: Geometry of a co-located PR where the reference and surveillance receivers are in the same physical location.

1.1.2 Separated Receivers

Another PR configuration, where the reference and surveillance channels are separated, is illustrated in Figure 1.4. In this geometry the receivers can be placed in separate locations. This allows the surveillance channel to be placed in a location shielded from the reference, but not the target echoes. Depending on the placement, this can be used to break direct Line of Sight (LoS) with the IoO, reducing the DSI power levels.

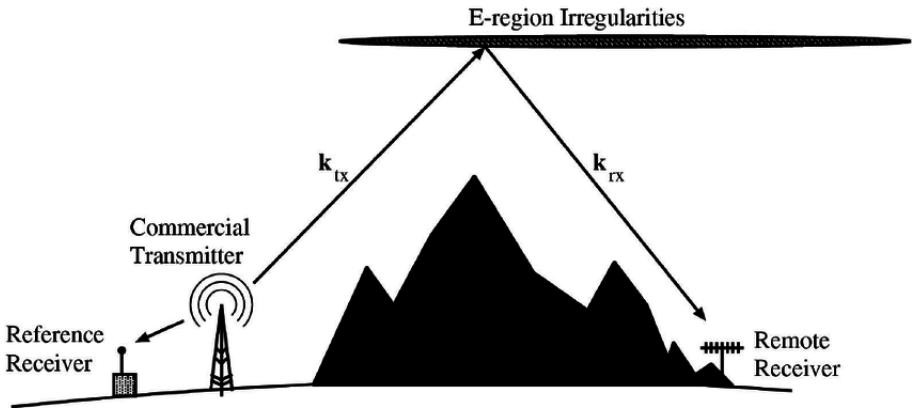

Figure 1.4: Geometry of a PR where the reference and surveillance receivers are in different physical locations.

1.1.3 Range and Doppler Resolution

Two important factors in radar performance are the range and Doppler resolutions. Ambiguity Range Doppler (ARD) maps are made up of range and Doppler bins and the size of these bins is defined by the corresponding resolution. The finer the resolution the more accurately the range or Doppler shift of the echoes can be measured. This is critical for accurately ranging and tracking target echoes in

space, relative to the radar. Equations 1.1 and 1.2 define the range and Doppler resolutions for a given signal respectively [8].

$$\Delta r = \frac{c_0}{2cos(\frac{\beta}{2})B} \tag{1.1}$$

Where Δr is the range resolution, c_0 is the speed of light, β is the bistatic angle, seen in Figure 1.5, and B is the bandwidth of the signal. The range resolution defines how accurately the PR can measure the position of a target in space. A finer range resolution indicates improved accuracy. This equation is a significant reason as to why the bandwidth of the transmitted signal is an important consideration when discussing potential IoO's.

$$\Delta f_D = \frac{1}{T} \tag{1.2}$$

Where Δf_D is the Doppler resolution and T is the integration interval. The Doppler resolution defines how accurately the Doppler shift caused by a target and, by extension the radial velocity of the target, can be measured.

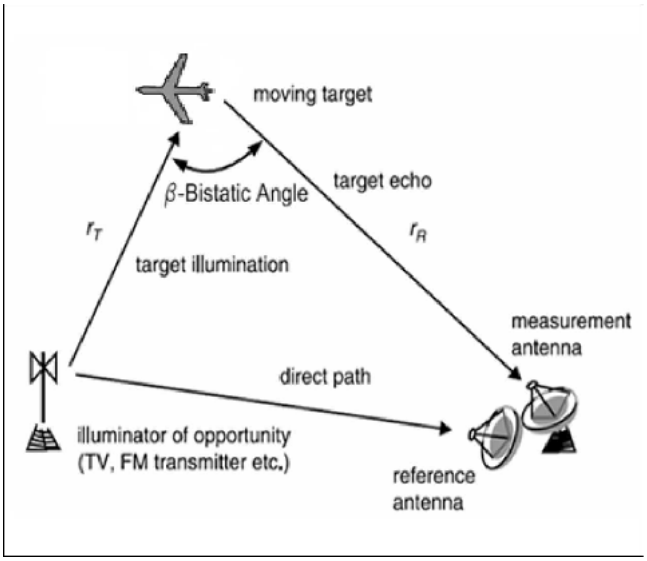

Figure 1.5: Geometry of a PR with labels for the purpose of calculation.

1.1.4 IOO Signals

An IoO comes from a pre-existing in the environment. In this work the relevant IoOs come from telecommunication infrastructure. Signals used for telecommunication are categorised as either analogue or digital based on whether the data being transmitted is discrete or not. For PR this distinction is useful in discussing the waveforms as radar signals. Analogue and digital signals have different advantages and drawbacks in the waveform being transmitted.

Analogue Signals

Analogue signals are continuous waveforms that are used for telecommunications by encoding information in a continuously changing quantity. For example Frequency Modulation (FM) signals use frequency modulation to encode information into the value of the instantaneous frequency of the signal. Amplitude Modulation (AM) is another example where information is encoded by varying the amplitude of the signal. Due to the varying frequency and high transmit power of FM signals, FM towers are often considered as IoO's for passive radar systems.

FM provides a signal with varying frequency which results in a range resolution acceptable for long range detection applications. The drawback of this is that the instantaneous bandwidth is inconsistent and the PR is dependant on the content of the transmission. When little to no content is being transmitted the bandwidth becomes extremely low, resulting in very poor range resolution [9].

OFDM Signals

In this thesis the digital signals considered are both Orthogonal Frequency-Division Multiplexing (OFDM) signals, resulting in similarities in the signal structure. OFDM signals allow for information to be encoded in the signal in multiple frequency bands. This is achieved by splitting the signal into frames which each have the same structure. Each frame is divided up into time slots and frequency bands to form subcarriers or symbols. By encoding certain symbolswith predefined and known values as signalling information, the signal can be reconstructed accurately at the receiver. In Digital Video Broadcasting — Second Generation Terrestrial (DVB-T2) each of these is known as a pilot and Long Term Evolution (LTE) makes use of both Reference Signal (RS) and Synchronisation Symbol (SS) symbols. These can be used to align the received signal in time and frequency as the value and position of these symbolss are known.

These symbols cause range and Doppler ambiguities in the Ambiguity Function (AF) and ARD map due to the correlation caused by their repetition in time and, for certain symbols, frequency. This causes false detections and can mask targets. These ambiguities become more significant as the integration interval is increased.

The advantage of these signals is that they have large bandwidths that remain consistent. This results in a consistently fine range resolution. The frame structure of these signals lends itself well to be processed using algorithms that divide the signal into pulses as the similarity of the frames prevents decorrelation between pulses.

1.2 Overview of Processing Chain

To exploit the advantages of each of these signal types and use them to mitigate the drawbacks, a streamlined processing pipeline capable of producing the ARD map for any signal in a generalised PR system is necessary. To do this there are two main steps in the processing chain that must be considered. These are the following:

- The cancellation algorithm.
- The range-Doppler processing algorithm.

In Figure 1.6 it can be seen that these are the parts of the general PR processing chain that often vary based on the signal transmitted by the IoO. For example, inverse filtering is designed to be used on OFDM signals and Conjugate Gradient Least Square (CGLS) is commonly used for analogue signals.

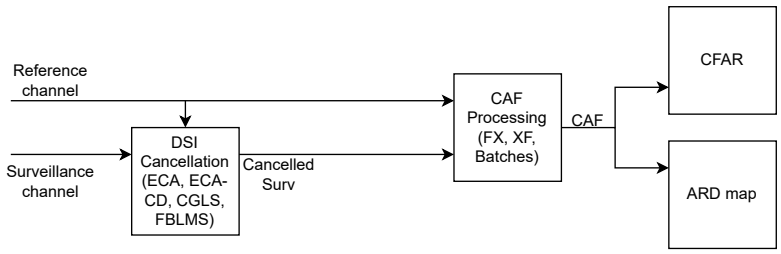

Figure 1.6: The general Processing Chain.

1.2.1 Cancellation Algorithms

To overcome the effect of the DSI and mitigate clutter in the signal a cancellation algorithm is necessary. Cancellation algorithms use the signal in the reference channel to filter out the DSI in the surveillance channel. The following algorithms are considered in this thesis:

- CGLS
- Extensive Cancellation Algorithm by Carrier/Doppler (ECA-CD)

These are further discussed in Chapter 3.

Other algorithms include Extensive Cancellation Algorithm (ECA), Extensive Cancellation Algorithm by Carrier (ECA-C), Singular Value Decomposition (SVD) and Frequency Domain Block Least Mean Square (FBLMS). The focus of this thesis is on ECA-CD and CGLS due to previous research demonstrating robust results using these algorithms [4, 10].

1.2.2 Range-Doppler Processing Algorithms

The range-Doppler algorithm produces what is known as the Cross Ambiguity Function (CAF). This can be used to visually display the ambiguities between the two input signals across range and Doppler shift axes. When the same signal is used as both signal inputs the algorithm produces an estimation of what is known as the Auto Ambiguity Function (AAF), or simply AF, which is useful for signal analysis. Another term for the CAF is the ARD map. For the purposes of this thesis, CAF refers to the numerical matrix produced while the ARD map refers to the Matlab plot produced using the CAF.

The following range-Doppler processing algorithms are considered in this dissertation [4, 11, 3]:

- Fourier transform - Cross multiply (FX)
- Cross multiply - Fourier transform (XF)
- Inverse Filtering
- Batches Processing

These are further discussed in Chapter 3.

1.3 Motivation

The objectives of this research are the following:

- Design a generalised PR processing chain that works for both FM and OFDM signals.
- Optimise the chain by selecting algorithms based on a balance of effectiveness and processing efficiency.
- Remove unnecessary options to improve usability.

1.4 Objectives

The primary objective of this work was to demonstrate a generalised processing pipeline that can produce an ARD map for any potential analogue, such as FM, or OFDM based, such as DVB-T2, IoO.

This provides a few key benifits:

- The hardware requirements for the system will be reduced.
- The code-base is significantly reduced and code maintenance is made easier. This is more useful as the number of different illuminators used is increased.
- The system can be more easily deployed.

In support of the main objective, additional objectives of this work were to:

- Demonstrate that Frequency Domain (FD) based processing, specifically ECA-CD, can be used to effectively process traditional analogue signals such as FM radio.
- Demonstrate that LTE signals can be an effective PR IoO when the pilot equalisation technique previously developed for DVB-T2 PR is adapted for the LTE signal.

1.5 Scope & Limitations

The processing chain considered in this work is designed to output a separate ARD map for each IoO used. Combining the final results is non-trivial due to the differences caused primarily by the sampling rates necessary and therefore the bandwidth of the different signals and their carrier frequencies. Due to these reasons, a combined ARD or a universal tracker that takes these different signals as inputs was not considered as part of this body of work.

1.6 Thesis Outline

Chapter 2 of this thesis provides a review of existing PR literature. It first covers research in the PR field as a whole and continues with literature specifically relevant to developing and streamlining the processing chain and the IoO signals.

Chapter 3 outlines the structure of the processing chain, the specific of the considered algorithms, the usable combinations and the algorithms finally used.

In Chapter 4 the FM aspect of this research is covered. A review of the FM waveform and the typical processing chain used in FM passive radar is discussed. Research into using ECA-CD as a cancellation algorithm for FM signals is presented.

Chapter 5 begins by discussing the general OFDM structure and equations for where ambiguites are expected in the ARD map. This is followed by the LTE section which starts with a comprehensive overview of the LTE signal. investigation into the spectrogram and ambiguites is presented, followed by the methodology behind the equalisation technique used. The LTE section concludes with the results of investigating the use of LTE for PR application. The final section in this chapter covers the DVB-T2 signal. An overview of the signal is given, followed by a discussion on the ambiguities in the ARD map.

Chapter 6 presents the results when targets are simulated in all three signal types. The results demonstrate that the processing chain can effectively process all three signals.

Chapter 7 concludes this thesis by presenting the objectives achieved, conclusions of the research and goes on to discuss future work.

Chapter 2

Literature Review

This chapter discusses the literature relevant to PR and more specifically to the research presented in this work. The chapter starts by discussing the early research done in PR starting in the 1930s. This is followed by literature on FM PR, DVB-T2 PR then LTE PR system. The chapter concludes with a review of hybrid PR systems in different stages of completion.

2.1 Early Passive Radar Research

PR as a concept has been around for a long time, with the first experiments being performed before World War II (WWII). The Daventry experiment which was performed in 1935 and used the British Broadcasting Corporation (BBC) broadcast as an IoO was the first demonstration of PR [12]. During WWII other PR systems, such as Klein Heidelberg, were developed by the German forces to exploit the British Chain Home radar transmitter [13]. After the war, interest in PR dwindled due to the performance of monostatic, active systems and the limitations in implementing PR at the time [14]. With the later increased availability and improvement of computing resources such as General Purpose Graphics Processing Units (GP-GPUs), Software Defined Radio (SDR) and Analogue-to-Digital Converters (ADC) research into PR has seen increased interest which started in the 1980s [14].

An early paper in the renewed research was the work performed by Griffiths and Long [15] where analogue Television (TV) broadcasts were used. The Crystal Palace transmitter in South London was chosen as the IoO. The goal was to detect aircraft taking off and landing at Heathrow airport. It was found that the autocorrelation function of the analogue TV had high sidelobes and course range resolutions. The signal also exhibited major ambiguities at 9 6km and it's integer multiples. Additionally, the ADC's at the time were limited to 8 bits resulting in a 48 dB dynamic range. With the integration gain being limited to a maximum equal to the dynamic range, this was insufficient for resolving targets. This conclusion is supported by [16].

Griffith's et al. investigated exploiting a Synthetic Aperture Radar (SAR) satellite as an IoO in papers released in 1992 and 2002 [17, 18]. Expected signal levels, ambiguities and the expected performance of a system using a stationary ground receiver were described.

in 1997 Sahr and Lind described a method to exploit FM broadcasts near 100 MHz for remote sensing of the upper atmosphere [19]. In this paper, novel cancellation methods were discussed and the usefulness of the AF to analyse radar waveforms was described. These findings were later reaffirmed by Griffiths and Baker in 2005 [20]

Two 2005 papers published by Griffiths and Baker discussed the theoretical performances when exploiting different waveforms. The Part 1 paper examined FM, Digital Audio Broadcasting (DAB) and Global System for Mobile communication (GSM) base stations as IoO's [21]. The DSI was discussed, as well as several methods to suppress the DSI. Part 2 of the paper analyses FM, DAB, GSM and analogue TV as IoO's [20].

2.2 FM research

In developing countries FM infrastructure tends to be a prevalent method of communication. In South Africa, FM infrastructure provides widespread coverage. Therefore a large amount of PR research at University of Cape Town (UCT) has been focused on FM infrastructure as an IoO [22, 23, 24, 25, 5, 26, 27, 28, 29, 30].

In 2005 a paper by Howland et al. [31] reported on results for a FM PR using an IoO in Lopik, 50 km from the receiver. Howland noted the DSI as the main obstacle in target detection and emphasised the importance of effective 'interference rejection' [31] now commonly achieved using cancellation. A single channel was used, limiting the bandwidth to that of a single FM channel. as a result the range resolution came to roughly 2 km, however, targets were tracked up to 150 km away.

Similar conclusions about the usefulness of FM PR for long-range applications are well documented by multiple sources [32, 33, 23]. This is widely agreed to be due to the high transmission power and long wavelengths providing a useful signal for long-range coverage.

FM PR is limited by the varying instantaneous bandwidth which depends on the content being transmitted, leading to inconsistent system performance [9]. To address this, Lauri et al. investigated using multiple FM channels. It was found that silence was the worst for FM PR performance, while voice and music were useful.

Bongioanni et al. analysed a FM PR system that utilised multiple FM channel [34]. The authors found that by recording six channels simultaneously and adding one or more channels incoherently, the system performance could be improved. The authors attribute this to the increased robustness against the effects of the time varying bandwidth of a single narrowband channel.

Żywek et al. developed a real-time method of transmitter selection based on short-term bandwidth analysis in 2021 [35]. In this paper, the authors present an equation to estimate the effective bandwidth of a given FM interval.

2.3 DVB-T2 Research

OFDM signals have properties that are particularly useful for radar applications. It should be no surprise that as the deployment of DVB-T2 has increased, research into DVB-T2 as an IoO has also increased. Compared to other OFDM signals, DVB-T2 has a high transmit power due to the required coverage and is being deployed in many countries around the world [36].

There have been many demonstrated PR systems making use of the predecessor of DVB-T2, Digital Video Broadcasting – Terrestrial (DVB-T) [37, 38, 39, 40, 41, 42, 43, 44]. As DVB-T2 became more

widespread and replaced DVB-T, PR systems exploiting DVB-T2 emerged [45, 46, 47, 48, 49, 50, 51].

DVB-T2, as with other OFDM signals, provides several advantages for PR. Digital signals have high bandwidth which provides fine range resolution. The bandwidth is also constant, providing stable performance. The signaling in OFDM signals is also useful in allowing the re-modulation and de-modulation scheme [52, 53, 54] referred to as demod-remod. Demod-remod allows for the signal to be reconstructed as a perfect reference. This is made possible by the open standard [55].

Various sources have discussed the demod-remod process in the context of OFDM based PR for both DAB [52] and DVB-T [56, 44]. O'Hagan et al. demonstrated using the demod-remod process in the DVB-T2 context [47]. The authors discussed pilot blanking and equalisation. They noted that the pilots are by a factor of 7/4 and therefore setting the pilots to $(\frac{4}{7})^2$ of their original level results in the pilots being normalised. The results of this research indicated that equalising the pilots clearly removed the ambiguities they cause.

In his 2019 PhD thesis, Paine demonstrated the effectiveness of various jamming techniques on FM and DVB-T2 PR [3].

2.4 LTE Research

LTE signals have a bandwidth range of 1.2 to 20 MHz, a wide frequency band and the resulting range and Doppler resolutions are good. These factors, along with the OFDM nature of the signal make it deirable as a signal for PR [57, 58]. LTE PR have been research for various applications [59]. A prominent application is the detection and tracking of people, particularly in cities [60, 61].

In 2013 Sallah et al. [58] investigated the feasibility of LTE as an IoO for PR. For a LTE signal with a 20 MHz bandwidth the range and Doppler resolutions were found to be 75 m and 0.11 m/s. The authors concluded that this makes the LTE signal desirable as and IoO.

In 2014 Evers and Jackson [62] made use of LTE, DAB and Digital Video Broadcasting (DVB) in experiments using the OFDM IoO's in a SAR system [63]. In the same year, the authors released a paper analyzing the LTE signal using the AAF. They noted that the features of the LTE signal result in reduced performance, however, allow for a partially matched filter to be easily developed using the predefined standard [64].

Sardar et al. [65] used an experimental setup known as LTE-CommSense to determine if the system could distinguish objects in an outdoor environment. The objective of LTE -CommSense was to detect environmental changes due to the presence of objects. THe authors concluded that the CommSense could be used in an outdoor environment to detect targets and distinguish them from one another.

Blazquez-Garcia et al. [66] proposed a novel Railway Network Surveillance PR using the Long Term Evolution-Railway (LTE-R) signal being implemented along railways in various European, North American and Asian countries as an IoO. The purpose of this system is to detect intrusions along the railway and communicate this to railway operators. This is due to the high speeds of trains increasing the risk of collision. The system is estimated to be able to detect pedestrians and drones within a few kilometres. Notably, the system is estimated to have a 90% detection probability at up to 15 km from

the receiver for a car with an Radar Cross-Section (RCS) of $2\,m^2$.

2.5 Processing Chain

Tong's 2014 thesis demonstrated a real-time processing chain DSI-cancellation for PR for commercial hardware [4]. The DSI-cancellation used is CGLS and the CAF produced uses what Tong describes as XF. XF will be described in further detail in section 3.3.1. Tong outlines the details of a complete PR processing chain including both the cancellation and range-Doppler processing steps.

Zhao et al. proposed an advanced ECA algorithm known as ECA-C [67]. This algorithm applies ECA to the temporal evolution of each OFDM carrier, however it only suppresses the sidelobes caused by clutter without Doppler shifts. Schwark later addressed this with ECA-CD.

A 2016 paper by Schwark et al. [68] proposed ECA-CD as an improvement on the ECA-C and ECA algorithms. This algorithm is designed to make use of the OFDM signals structure in FD processing foe efficient DSI-cancellation on these high bandwidth signals. The algorithm expands the clutter subspace used in ECA-C by two copies of the reference carrier. This requires the signal to be in the FD.

In 2020, Schüpbach et al. performed a qualitative analysis to determine whether ECA-CD is an effective cancellation method when applied to an FM signal [10]. The authors concluded that ECA-CD achieves similar performance to CGLS when applied to FM if the range-Doppler processing used is the Batches algorithm.

Petri et al. [69] performed a performance analysis on the FMCW-like Batches approach to producing a CAF. The result of their work demonstrated that the Batches approach produces an approximation of the CAF with comparable performance to a complete CAF calculation, but with a significantly lower computational load. The authors reported a 96% reduction in the computational load of creating the CAF.

2.6 Hybrid Passive Radar systems

In 2011 Kuschel et al. [70] proposed a hybrid PR system making use of FM, DVB-T and DAB as IoO's. The system made use of FM to detect the target and by using the FM Doppler information, a track-before-detect approach was used for the DVB-T and DAB signals to provide high-resolution tracking.

Also in 2011, Cassidian developed a mobile PR system that exploited FM, DAB and DVB-T for various surveillance applications [33]. The authors propose that the system has a 200 km detection range. Targets could be located with an accuracy of 100 m. The further work that needed to be performed on this system was fusing the data produced by the different receivers.

2018 saw Peralex demonstrate a hybrid FM and DVB-T2 based PR [71]. The system was designed to be deployed in the Square Kilometer Array (SKA) site in the Northern Cape province of South Africa [71]. The goal is to track targets in the airspace around the site without damaging the highly

sensitive radio telescope receiver on the site. The authors demonstrated that target detection could be performed with both signals providing a robust PR system [71].

In his 2019 PhD thesis, Paine demonstrated the effectiveness of different jamming techniques on FM and DVB-T2 PR [3]. Paine's conclusion indicates that jamming is a real risk for PR systems. This further reinforces the need for IoO diversification in PR systems.

Chapter 3

Processing Chain

This chapter provides an overview of the processing chain followed by detailed descriptions of each element. The descriptions of the DSI cancellation and range-Doppler processing algorithms are given, followed by method of target simulation and pilot equalisation. The chapter closes by describing the potential combinations of algorithms.

3.1 Overview

The generalised processing chain is illustrated in Figure 3.1 below. For digital signals, the reference channel first has the demod-remod process applied to it and the surveillance channel is aligned in time to the reference. After cancellation, the reference channel has pilot equalisation applied to it as illustrated in Figure 3.3 The pre-processed signals or the raw signal in the FM case then have a cancellation algorithm applied to them. The reference and cancelled surveillance signal are used as the input to the CAF making algorithm. The resulting CAF is then used to make an ARD map and the result from one or more frames can used in a Constant False Alarm Rate (CFAR) algorithm for target detection.

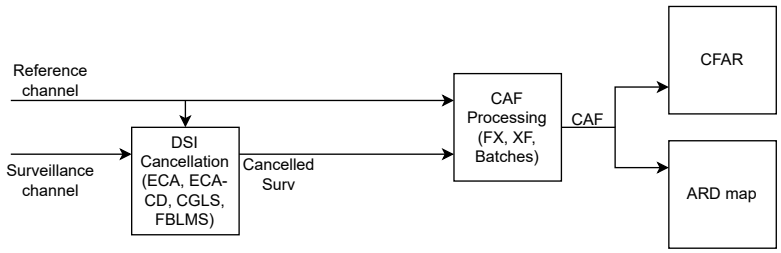

Figure 3.1: General Processing Chain.

The demod-remod processing is specific to each digital signal. Parameters such as sampling rate, integration time per frame and the center frequency of the signal are unique to each signal type. Therefore, in a generalised PR processing chain the primary processing steps that need to be considered are the cancellation and range-Doppler algorithms. These are described further in the following subsections.

3.2 DSI Cancellation Algorithms

The DSI is a significant obstacle in target detection, having a significantly higher power level than the target echoes. To overcome this challenge, DSI cancellation is necessary and the DSI cancellation algorithm is an important factor in the performance of a PR processing chain.

3.2.1 Conjugate Gradient Least Squares - CGLS

CGLS is an iterative algorithm based on the conjugate gradient technique and makes use of least squares to minimise the $S_{dsi} = A_x$ function. By applying a set number of iterations the execution time will be fixed. A balance of time efficiency and and sufficient DSI reduction must be managed. The relatively constant DSI levels often present in systems where the transmitters and receivers are static, the number of iterations can be estimated using trial and error [4]. In this case the DSI reduction will be sufficient while the latency of the processing chain is made constant. To reduce the computational load, the weight from the previous frame can be used in the next frame to reduce the number of necessary iterations [4]. However, this method requires relative similarity between frames, making the processing chain less capable of handling significant changes in the signal, for example if the signal is being jammed [3].

CGLS is a rigorous Time Domain (TD) cancellation algorithm. Due to it's iterative nature the computational load becomes significant for signals with a high number of samples in each Coherent Processing Interval (CPI).

3.2.2 ECA-CD

ECA-CD is an enhanced ECA proposed by Schwark [68]. ECA is an effective algorithm, however it projects the surveillance signal into a subspace orthogonal to the reconstructed signal of each scatterer. This becomes more computationally expensive as the number of scatterers increases.

A technique known as ECA-C was proposed by Zhao et al. [67], which makes use of the structure of OFDM signals. In ECA-C, ECA is applied to the temporal evolution of each OFDM carrier [67]. ECA-C only suppresses the sidelobes caused by clutter without Doppler shifts.

To address sidelobes caused by multipath clutter with a Doppler shift, a technique known as ECA-CD was proposed by Schwark et al. [68]. In ECA-CD the clutter subspace in ECA-C is expanded by two copies of the reference carrier, each frequency shifted by the Doppler frequencies as is explained by Shwark [68]. This algorithm requires the signal to be in the FD.

By applying an Fast Fourier Transform (FFT) to the signal before making use of ECA-CD and applying an Inverse Fast Fourier Transform (IFFT) afterward, the algorithm can be used on a TD signal. ECA-CD is computationally efficient, allowing for low processing times for both FD and TD signals, while still being an effective cancellation algorithm.

With the findings in Chapter 4 it was shown that ECA-CD is effective not only for use with analogue signals, but also TD signals. As a result ECA-CD was the chosen DSI algorithm for the generalised processing chain.

3.3 Range-Doppler Processing Algorithms

This step in the processing chain makes use what is known as the CAF. The CAF is the range-Doppler cross correlation function between the reference and surveillance signals. It is defined by Equation 3.1 for a bistatic delay and Doppler shift, τ and f_d respectively.

$$\Phi(\tau, f_d) = \int_{-\infty}^{\infty} x_s(t) x_r^*(t+\tau) e^{-j2\pi v f_d t} dt \tag{3.1}$$

Where x_r and x_s are the TD reference and surveillance signals respectively. Note that * indicates the complex conjugate of the signal.

For a CPI that is both finite and in discrete time, a discrete form of this expression is requires. Equation 3.2 is the finite, discrete form of Equation 3.1 squared. It is squared to implement square law detection [4].

$$|C(m,k)^2 = |\sum_{n=0}^{N_s-1} f(n,m) e^{j2\pi kn/N_s}|^2 \tag{3.2}$$

Where m is the time delay in the form of a number of samples and k is a Doppler bin index. N_s is the number of samples that make up the length of the CPI.

The main methods of making use of the FFT to speed up the process are XF and FX algorithms [4]. The names of these algorithms are borrowed from a radio astronomy naming convention. 'F' refers to the Fourier Transform or FFT in this case. 'X' refers to point-wise cross multiplication. The order of 'X' and 'F' in the name of each algorithm simply refers to the order that each of the operations is performed in the algorithm.

The 'FMCW-like' [11] or 'Batches' [72] method divides the CPI into smaller batches. The cross-correlation of the reference and surveillance in each batch is used to produce the CAF. This algorithm is computationally efficient, however, it may have errors under certain conditions.

3.3.1 Cross Multiply - Fourier Transform (XF)

The Digital Fourier Transform (DFT) in Equation 3.3 below is similar to one of the terms in Equation 3.2.

$$F(k) = \sum_{n=0}^{N_s=1} s(n) e^{-j2\pi kn/N_s} \tag{3.3}$$

Where s is the discrete time signal being transformed, k is the discrete frequency bin number and N_s is the number of consecutive samples that are being transformed. To relate Equations 3.2 and 3.3 we can use the function in Equation 3.4 [4].

$$f(n,m) = s_s(n){s_r}^*(n+m) \tag{3.4}$$

Where n is the sample number and m is the delay. With this substitution in mind and because m can be considered constant in the expression, Equation 3.2 can also be expressed as the following.

$$|C(m,k)^2 = |DFT(-k, \mathbf{f}(m))|^2 \tag{3.5}$$

Where $\mathbf{f}(m)$ is a function that returns a vector with n values, for the full CPI. The DFT operator performs a DFT on the vector for Doppler bin k. The negative k is due to the sign difference in the exponent between Equations 3.2 and 3.3. By making use of an FFT in place of the DFT the computational efficiency of the algorithm can be improved, resulting in Equation 3.6.

$$|C(m,k)^2 = |FFT(\mathbf{f}(m))|^2 \tag{3.6}$$

The k term is no longer necessary as the FFT calculates all frequencies from $\frac{-f_s}{2}$ to $\frac{f_s}{2}$ where f_s is the sampling frequency. The resolution of each Doppler bin is $\frac{1}{T_{CPI}}$ Hz where T_{CPI} is the CPI length in seconds.

This can be further sped up by applying a low pass filter to the signal and decimating it. Howland et al. [31] achieved a reduction in complexity in the order of 15 times based on this method.

3.3.2 Fourier Transform - Cross Multiply (FX)

The FX algorithm makes use of the cross-correlation theorem. The theorem states that performing a cross-correlation in the TD is equivalent to performing a point-wise conjugate multiplication in the FD as can be seen in the Equation 3.7 Fourier Pair:

$$Corr(f,g) \longleftrightarrow F^*.G \tag{3.7}$$

Where $Corr$ is the cross correlation operation, . indicates point-wise multiplication and * indicates the complex conjugate. The lower case f and g indicate two TD signals and the upper case F and G are the FD, Fourier transforms of the aforementioned TD signals.

The FX algorithm takes the FFT of both the reference and surveillance channels and conjugates the surveillance. The corresponding bins between each channel is multiplied and the IFFT of the result is taken.

While the XF algorithm calculates all Doppler bins and a specific number of range bins, the FX algorithm is the reverse. The FX algorithm calculates all range bins up to the maximum delay of the CPI or $N_s - 1$ where N_s is the total number of samples in the CPI.

3.3.3 Inverse Filtering

Inverse filtering is a range-Doppler processing technique that exploits the nature of OFDM signals for computational efficiency. This is achieved by effectively 'normalising' the surveillance channel in relation to the reference channel [3]. Consider the following representation of the direct signal received:

$$s_{ds}(t) = e^{i2\pi f_c t} \sum_{n=0}^{N-1} [A_n e^{i\Phi n} e^{i2\pi(-\frac{BW}{2}+n\frac{BW}{N-1})t}] \tag{3.8}$$

Where BW is the total bandwidth of the active carriers, N is the number of active carriers, f_c is the carrier frequency of the signal and $A_n e^{i2\Phi n}$ is the complex amplitude of carrier n. Target echoes in the signal will be time delayed copies of the representation in 3.8 in the form:

$$\begin{aligned} s_{echo}(t) &= s_{ds}(t - t_d) \\ &= e^{i2\pi f_c(t-t_d)} \sum_{n=0}^{N-1} [A_n e^{i\Phi n} e^{i2\pi(-\frac{BW}{2}+n\frac{BW}{N-1})(t-t_d)}] \end{aligned} \tag{3.9}$$

Where t_d is the echo delay defined as:

$$t_d = \frac{R_0}{c} + \frac{v_{bis}}{c} t \tag{3.10}$$

Where R_0 is the difference in bistatc range at symbol start, v_{bis} is the bistatic velocity measured from the echo and c is the speed of light. The baseband representations of Equations 3.8 and 3.9 are:

$$s_{ds,bb}(t) = \sum_{n=0}^{N-1} [A_n e^{i\Phi n} e^{i2\pi(-\frac{BW}{2}+n\frac{BW}{N-1})t}] \tag{3.11}$$

and

$$\begin{aligned} s_{echo,bb}(t) &= e^{-i2\pi f_c t_d} \sum_{n=0}^{N-1} [A_n e^{i\Phi n} e^{i2\pi(-\frac{BW}{2}+n\frac{BW}{N-1})(t-t_d)} \\ &= e^{-i2\pi f_c \frac{R_0}{c}} e^{-i2\pi f_c \frac{v_{bis}}{c} t} \sum_{n=0}^{N-1} [A_n e^{i\Phi n} e^{i2\pi(-\frac{BW}{2}+n\frac{BW}{N-1})(1-\frac{v_{bis}}{c})t} \cdot e^{-i2\pi(-\frac{BW}{2}+n\frac{BW}{N-1})\frac{R_0}{c}}] \end{aligned} \tag{3.12}$$

respectively.

The time delay t_d has the following effects:

- A Doppler shift is induced, $e^{-i2\pi f_c \frac{v_{bis}}{c} t}$.
- The phase term determined by the bistatic distance, $e^{-i2\pi f_c \frac{r_0}{c}}$, is introduced.

- A phase shift that is directly proportional to the bistatic distance of the target is introduced to each sub-carrier by the term $e^{-i2\pi(-\frac{BW}{2}+n\frac{BW}{N-1})\frac{R_0}{c}}$

Inverse filtering exploits the sub-carrier phase shift for range processing.

The echo signal is normalised in the FD by dividing complex amplitudes of the echo signal spectrum, element wise, by the complex amplitudes of the direct signal spectrum as in Equation 3.15.

$$s_{ds,bb}(k) = A_k e^{i\Phi k} \tag{3.13}$$

$$s_{echo,bb}(k) = A_k e^{i\Phi k} \cdot e^{-i2\pi f_c \frac{R_0}{c}} \cdot e^{-i2\pi(-\frac{BW}{2}+k\frac{BW}{N-1})\frac{R_0}{c}} \cdot sinc(\frac{\pi f_c N}{BW} \cdot \frac{v_{bis}}{c}) \tag{3.14}$$

$$s_{norm,bb}(k) = e^{-i2\pi f_c \frac{R_0}{c}} \cdot e^{-i2\pi(-\frac{BW}{2}+k\frac{BW}{N-1})\frac{R_0}{c}} \cdot sinc(\frac{\pi f_c N}{BW} \cdot \frac{v_{bis}}{c}) \tag{3.15}$$

This is where the term inverse filtering is derived from.

The result is a rotating phasor where the speed of rotation is directly proportional to the bistatic range of the echo. Ignoring Inter-Signal Interference (ISI), the range processing is achieved using the DFT:

$$S_{range}(p) \triangleq DFT(S_{norm,bb}) \tag{3.16}$$

S_{range} is at the maximum amplitude when:

$$p_{max} \approx BW\frac{R_0}{c} \tag{3.17}$$

Successful processing of adjacent OFDM symbols yield similar results, with on the phase differing due to the change in R_0.

$$S_{range,symbol(y+1)} \approx S_{range,symbol(y)} \cdot e^{-i2\pi f_c \frac{R_\Delta}{c}} \tag{3.18}$$

Where R_Δ is the change in the bistatic range. Arranging subsequent range lines into the rows of a matrix, therefore, creates an additional rotating phasor down each of the columns:

$$\begin{aligned} s_{Doppler}(p,y) \triangleq S_{range,symbol(y)}(p) \\ S_{range}(p) \cdot e^{-i2\pi f_c \frac{R_\Delta}{c} y} \end{aligned} \tag{3.19}$$

In this case the speed of rotation is determined by the term $e^{-i2\pi f_c \frac{R_\Delta}{c}}$. The DFT of the matrix columns (slow time) produces the CAF:

$$CAF(p,q) = DFT(s_{Doppler}(p,y)) \tag{3.20}$$

Where the maximum amplitude of the CAF occurs when:

$$q_{max} = \frac{f_c R_\Delta N_{sym}}{c} \tag{3.21}$$

Where N_{sym} is the number of consecutive OFDM symbols processed to produce the CAF.

The inverse filtering technique is heavily reliant on the OFDM nature of the signal and the FFT length directly limits the maximum unambiguous range and Doppler of the system. For large symbol lengths in particular the maximum unambiguous Doppler is drastically reduced.

Furthermore, the reliance on the OFDM nature of the signal makes inverse filtering unsuitable for range-Doppler processing of analogue signals.

3.3.4 FMCW-like/Batches

The Batches algorithm was described by Griffiths et al. [11] and was expanded into a more general form by Petri et al. [72] where a 96% reduction in the computational load to create a CAF is demonstrated. The algorithm divides the TD CPI into smaller intervals known as batches. The cross-correlation of the reference and surveillance in each batch is stored as the rows of a matrix. To produce and approximate CAF, a FFT is applied to the columns of the matrix.

By making use of these batches this algorithm can speed up the processing required to create the CAF that, by visual inspection, are the same as those produced by other methods. This is particularly useful for applications where real-time processing is required or for site assessments.

A potential drawback is discussed by Petri et al. [72]. There is a phase shift error caused by correlating the reference which isn't Doppler shifted with the Doppler shifted reflections. This error increases with the length of the batches as well as larger Doppler shifts. Tong [4] suggests using Equation 3.22 when deciding on a batch size to mitigate this error.

$$\Delta f_{dmax} \times T_{batch} \ll 1 \tag{3.22}$$

Where Δf_{dmax} is the maximum Doppler shift expected from targets and T_{batch} is the time length of each batch.

The batches algorithm is a an efficient and effective range-Doppler processing algorithm for TD and FD signals. Additionally, the pulsed nature of ECA-CD is similar to the batches of the Batches algorithm. By making the number of ECA-CD pulses and batches equivalent, the amount of processing required between the two algorithms can be reduced. For these reasons, Batches was chosen as the range-Doppler processing algorithm for the generalised processing chain.

3.4 Target Simulation

To test the processing chain it is necessary to demonstrate that it works for all three signals. To do this targets need to be present in the data used. Furthermore, due to a potential application of this processing chain being a PR making use of multiple IoO's concurrently, results for signals of each type with the same targets present are desired. In the absence of real-world data with the desired scene, simulating targets in prerecorded data is the next best approach. Figure 3.2 illustrates the processing chain with target simulation included.

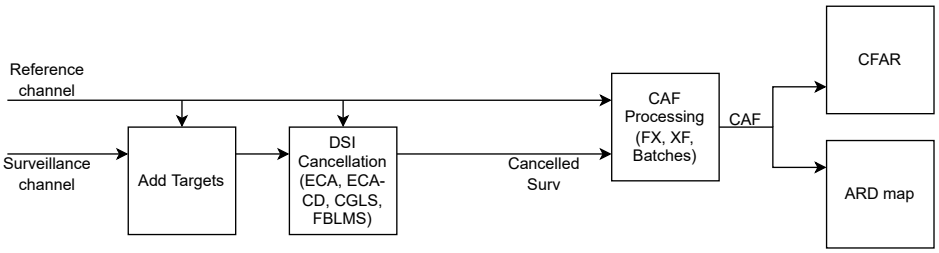

Figure 3.2: Generalised processing chain with target simulation.

To simulate targets in Matlab a function was used to insert the targets. The function takes an array of targets, the surveillance channel and the reference channel as inputs. The targets in the array have their distance from the receivers, Doppler shift and Signal to Noise Ratio (SNR) as parameters. The function makes a copy of the reference, delays the signal according to the distance, shifts the frequency according to the Doppler shift and reduces the signal power according to the SNR. These copies are then added to the surveillance channel.

The calculation used to generate the target echoes is as follows:.

$$\vec{targetSignal} = ((A \times \vec{refChannelData})' \cdot e^{2\pi i \times DopplerShift \times \vec{timeDelay}})' \tag{3.23}$$

Where A is the signal amplitude, defined as:

$$A = 1^{SNR} \times SurvDataRMS \tag{3.24}$$

and $\vec{timeDelay}$ is the time delay applied to each data point, defined in Matlab as:

$$\vec{timeDelay} = 0 : 1/fs : (length(\vec{survData}) - 1)/fs \tag{3.25}$$

Where fs is the sampling frequency.

3.5 Pilot Equalisation

Dealing with ambiguities caused by pilots is a necessary step when making use of an OFDM signal as an IoO. Therefore a technique known as pilot equalisation was used for both LTE and DVB-T2. These differ slightly for LTE and DVB-T2 depending on the specific OFDM structure and pilot levels. In general, however, this technique simply multiplies the pilots with a value that reduces them to the

power level of the data carriers. The complete processing chain with pilot equalisation included is illustrated in Figure 3.3.

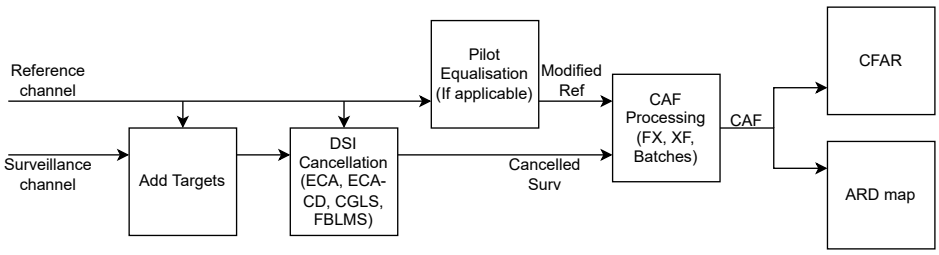

Figure 3.3: Generalised processing chain target simulation and pilot suppression.

3.6 Description of Processing Combinations

The main decisions to be made in the processing chain are which cancellation algorithm and which range-Doppler processing algorithm to use. Therefore it is important to understand which combinations can be used. Without additional use of FFT's and IFFT's TD algorithms are only effective on TD signals and the same applies to TD algorithms and signals. Figure 3.4 below illustrates this.

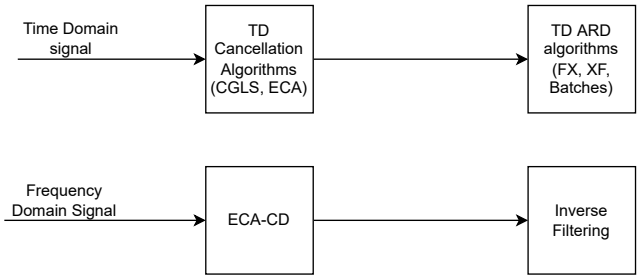

Figure 3.4: Illustration of the usable combinations of cancellation and range-Doppler algorithms.

By making use of FFT's and IFFT's the domain of the signal can be changed. This allows for combinations of TD and FD algorithms to be applied to both TD and FD signals. As a result almost any combination of cancellation algorithm and range-Doppler processing algorithm can be used. The only exception to this is Inverse Filtering. The implementation of Inverse Filtering in this processing chain requires the input to the algorithm to be in the matrix form expected from ECA-CD. Figure 3.5 below illustrates the usable combinations in the final generalised processing chain.

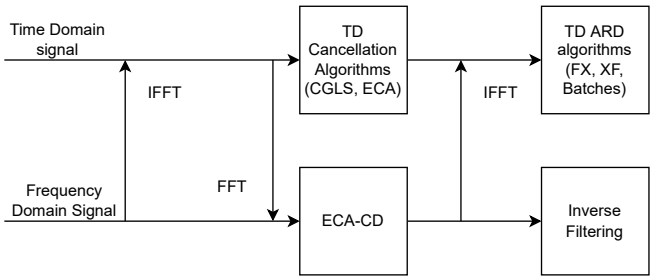

Figure 3.5: Complete illustration of the usable combinations of cancellation and range-Doppler algorithms.

Chapter 4

Analogue Signals

In this chapter the FM signal is described before an investigation into using FD processing in the form of ECA-CD on analogue signals such as FM is presented.

4.1 FM

4.1.1 Overview

FM signals are analogue signals that use varying instantaneous frequencies to encode information. As a result FM signals vary in bandwidth based on the content being transmitted and renders the signal useless when no content is being transmitted [9]. This can't be solved through processing, however, using an FM tower that is transmitting high bandwidth content consistently would mitigate these issues [9].

4.1.2 Signal Properties

In FM the baseband information signal, $m(t)$, modulates the frequency of the carrier signal. The FM signals that are broadcast are generated by making use of a Voltage Controlled Oscillator (VCO). The message signal is applied to the VCO to generate a sinusoidal carrier as an output. This carrier has a constant amplitude with an instantaneous frequency that is a function of $m(t)$. The function can be expressed mathematically as follows [73].

$$f_i(t) = f_c + K_{VCO} \times m(t) \tag{4.1}$$

Where $f_i(t)$ is the instantaneous frequency of the carrier signal, f_c is the centre frequency of the carrier and K_{vco} is the voltage-to-frequency gain of the VCO. When there is no message signal, the instantaneous frequency is equal to f_c.

The instantaneous frequency deviation of the carrier, Δf is equivalent to $K_{VCO} \times m(t)$. To determine the instantaneous phase, the integral of $f_i(t)$ is multiplied by 2π:

$$\begin{aligned}\theta_i(t) &= \int_0^t f_i(t)dt \\ &= \int_0^t 2\pi f_c dt + \int_0^t 2\pi K_{VCO} \times m(t)dt \\ &= 2\pi f_c t + 2\pi K_{VCO} \int_0^t m(t)dt\end{aligned} \tag{4.2}$$

The FM waveform can then be expressed as:

$$X_{FM}(t) = A_c cos(\theta_i(t)) \tag{4.3}$$

Where X_{FM} is the output FM waveform. By assuming that the initial phase is zero, this can be expanded to:

$$X_{FM}(t) = A_c cos(2\pi f_c t + 2\pi K_{VCO} \int_0^t m(t)dt) \tag{4.4}$$

The full mathematical model of $m(t)$ is as follows:

$$\begin{aligned}m(t) = C_0[L(t) + R(t)] \\ C_1 cos(2\pi \times 19kHz \times t) \\ C_0[L(t) - R(t)]cos(2\pi \times 38kHz \times t) \\ C_2 RDS(t) cos(2\pi \times 57kHz \times t)\end{aligned} \tag{4.5}$$

Where C_0 is the gain used to scale the amplitudes of the left and right channel, C_1 is the gain to scale the amplitude of the pilot tone at 19kHz and C_2 is the gain to scale the Radio Data System (RDS) subcarrier. This is to generate the correct modulation index, β. To simplify the calculation, an estimation can be made by modeling $m(t)$ as follows.

$$m(t) = A_m cos(2\pi f_m t) \tag{4.6}$$

Where A_m is the amplitude of the $m(t)$and f_m is the frequency of $m(t)$.

Substituting Equation 4.6 into Equation 4.4 results in:

$$\begin{aligned}X_{FM}(t) &= A_c cos[2\pi f_c t + \frac{k_{VCO} A_m}{f_m} sin(2\pi f_m t)] \\ &= A_c cos[2\pi f_c t + \frac{\Delta f}{f_m} sin(2\pi f_m t)] \\ &= A_c cos[2\pi f_c t + \beta sin(2\pi f_m t)]\end{aligned} \tag{4.7}$$

The modulation index, β, the ratio of Δf and f_m. β indicates the number of significant sidebands in the output spectrum. To demonstrate this the FM signal is presented in terms of the n^{th} order Bessel functions of the first kind.

$$X_{FM}(t) = A_c \sum_{n=-\infty}^{\infty} J_n(\beta)[\delta(f - f_c - nf_m) + \delta(f + f_c + nf_m m)] \tag{4.8}$$

By making use of Bessel function tables, the magnitude coefficient and number of sidebands of the FM signal can be determined.

Furthermore, Bessel functions can be used to determine the average power of an FM signal as:

$$P_{ave} = \frac{1}{2} A_c^2 \sum_{n=-\infty}^{\infty} J_n^2(\beta) \tag{4.9}$$

This is relevant because as the bandwidth is reduced, the number of sidebands necessary for transmission is reduced. Similarly, as the bandwidth increases so too does the number of sidebands necessary for transmission. What is important to note is that the integration gain achieved through matched filtering is directly proportional to the instantaneous bandwidth of the signal. An FM signal with a high modulation index and therefore a high instantaneous bandwidth is desirable. Therefore, the variable nature of the instantaneous bandwidth of FM signals can cause drops in the performance of the PR.

4.1.3 ECA-CD Applied to FM

The following is an extension of the work presented in [10]. To generalise and streamline the processing chain the cancellation algorithm used required careful consideration. While CGLS is robust, with OFDM it becomes computationally inefficient due to the high number of samples. Therefore an investigation into using ECA-CD on FM signals was carried out. The first step of this investigation was to confirm that ECA-CD is a functional DSI cancellation method for FM signals. To do this, a recorded FM signal with targets was processed using ECA-CD and the presence of the target was confirmed by inspection. A brief investigation into where the algorithm fails is demonstrated.

For ECA-CD to be a functional DSI cancellation method for an FM signal it must allow for target detection in an FM passive radar. To determine this the resulting CFAR plots when using CGLS and ECA-CD respectively were compared. The CFAR's are the result of 300s simulations with 1s CPI's.

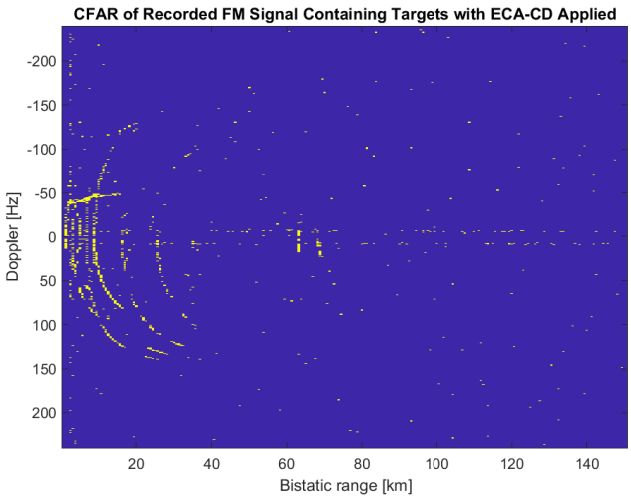

Figure 4.1: Combined CFAR of 100 consecutive 1s CPIs , ECA-CD applied.

Processing Parameters for Figure 4.1	
Signal	Recorded FM
Processing type	Batches
Processing Parameters	nPulses=500
Cancellation type	ECA-CD
cancellation parameters	nPulses=500
CPI samples	240e3(1s)
Number of CPIs	300
CFAR Algorithm	GOCA-CFAR
CFAR Window	4 reference, 5 guard
CFAR Dimension	Doppler
CFAR Threshold	$P_{fa} = 10^{-5}$

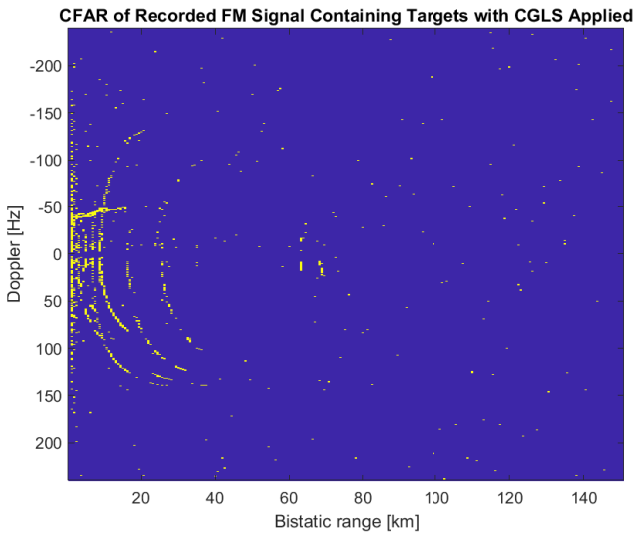

Figure 4.2: Combined CFAR of 300 consecutive 1s CPI's, CGLS applied.

Processing Parameters for Figure 4.2	
Signal	Recorded FM
Processing type	Batches
Processing Parameters	nPulses=500
Cancellation type	CGLS
cancellation parameters	nIterations=60, nSegments=16
CPI samples	240e3(1s)
Number of CPIs	300
CFAR Algorithm	GOCA-CFAR
CFAR Window	4 reference, 5 guard
CFAR Dimension	Doppler
CFAR Threshold	$P_{fa} = 10^{-5}$

Figures 4.1 and 4.2 are the CFAR's for the same signal with CGLS and ECA-CD applied respectively. By inspection, the CFAR's have detections of the same targets.

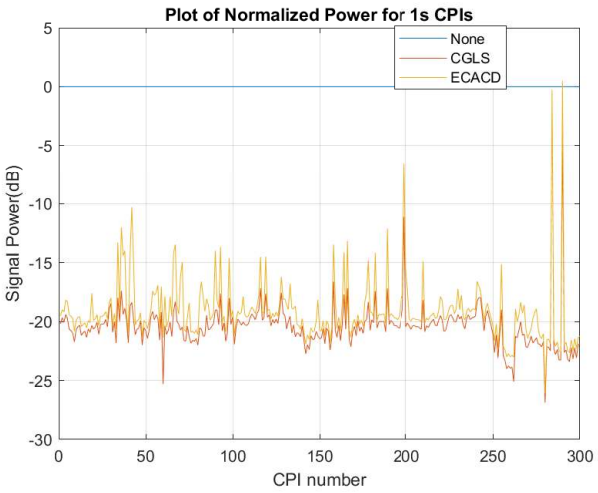

Figure 4.3: Plot of normalised CPI power.

Figure 4.3 plots the total power in the ARD maps at each CPI when using the different DSI cancellation methods normalised to the case with no cancellation. Each CPI is 1s long.

The peaks in the ECA-CD power plot correlate to CPI frames where ECA-CD fails as seen in Figure 4.3. This was hypothesized to be due to low bandwidth causing decorrelation.

To investigate the hypothesis a method of calculating the bandwidth of the FM signal during a given CPI was necessary. Zywek et al. [35] demonstrated that the Root-Mean-Square bandwidth calculation was consistent with the actual range resolution of the signal. This can be calculated using the following equation:

$$B \times A_{max} = \int A(f)df \tag{4.10}$$

Where B is the instantaneous bandwidth, $A(f)$ is the power spectral density of the signal and A_{max} is the maximum of $A(f)$.

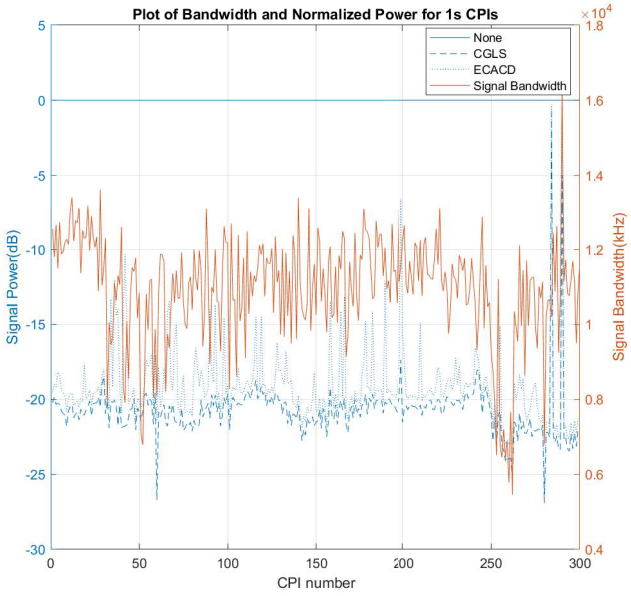

Figure 4.4: Plot of normalised power and signal bandwidth calculated for each CPI.

Figure 4.4 has the normalised powers plotted along with the bandwidth of the reference signal to test the hypothesis. This plot indicates no correlation between the two. This plot was then used to determine which CPI's are power peak cases and which are low bandwidth cases for further analysis

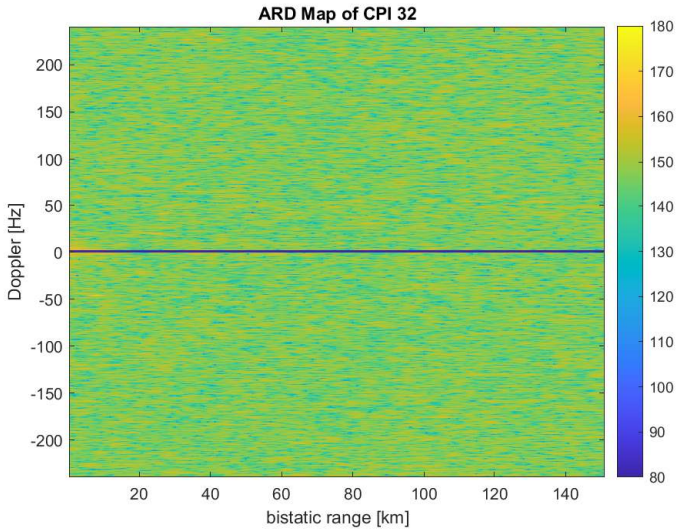

Figure 4.5: Plot of the ARD map for CPI 32, an example of a low bandwidth CPI

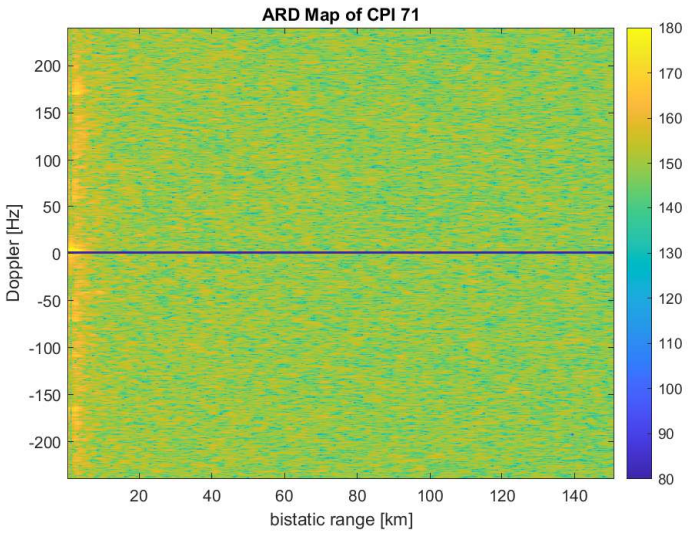

Figure 4.6: Plot of the ARD map for CPI 71, an example of a CPI with a normalised ECA-CD power peak.

The low bandwidth case in Figure 4.5 indicates a low Doppler resolution, but targets still appear to be present. This is what is expected when using a low bandwidth signal and no decorrelation is observed. The normalised power peak case in Figure 4.6 appears to be a different phenomenon. This does appear to be caused by decorrelation in the signal, however further investigation into the cause was not performed as it was beyond the scope of the investigation.

Target Simulation

The previous subsection demonstrates that ECA-CD is functional as a DSI cancellation algorithm for an FM passive radar. This does not mean it is effective or useful for this application. To determine it's effectiveness, the results of the ECA-CD and the CGLS cases were compared quantitatively. Specifically the probability of detection (P_d) and probability of false alarm (P_{fa}) were compared. To do this the exact position of the target in the ARD map had to be known. Therefore, reference signals and surveillance signals with simulated targets were used.

A radar simulator known as FERS was used to generate targets in a dataset [74, 75]. By using FERS, the positions, movement and other parameters of the illuminator, receivers and targets can be specified in a "fersxml" file.

Two targets were simulated separately. The first target starts at a point 10.3 km from the receivers and moves to a point 39 km from the receivers. The second target starts 37 km from the receivers and moves to a point 44 km from the receivers. Both move over the full 100 s at a constant velocity across a linearly interpolated path. For simplicity, the receivers were placed at the origin. Tables 4.1 and 4.2 have the coordinate positions of the first and second simulated targets respectively.

Target 1	X	Y	Z
Start Pos	2000	10000	1600
Final Pos	2000	39000	1600

Table 4.1: Table of the starting and ending position of the first target simulated over 100 s.

Target 2	Final X	Final Y	Final Z
Start Pos	2000	37000	1600
Final Pos	2000	44000	1600

Table 4.2: Table of the final position of the simulated targets after 100 s.

Broadband Noise Baseline

Due to the high bandwidth nature of broadband noise it was used to get baseline results for comparison with the FM results. The histograms in this section display the target detections and total detections achieved when using CGLS with 30, 40 and 60 iterations separately and when using ECA-CD. The P_{fa}, which is proportional to the total detections minus the target detections, is plotted for each case. The detections for each case were calculated by summing the total detections and target detections of 100 consecutive 1 s CFAR's.

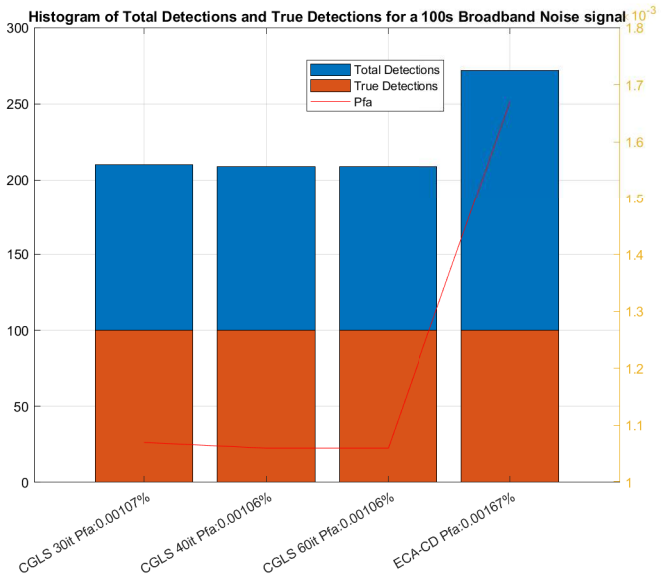

Figure 4.7: Histogram of the target detections and total detections for algorithms when used on a broadband noise signal.

Figure 4.7 indicates that for a broadband noise signal the results are the same for CGLS when using both a low and high number of iterations. This indicates that the algorithm requires a low number of

iterations to be effective on a broadband signal. When using both CGLS and ECA-CD, 100 target detections were made, indicating a high P_d. The P_{fa} for ECA-CD is high at 0.00167% when compared to the CGLS value of 0.00107% .

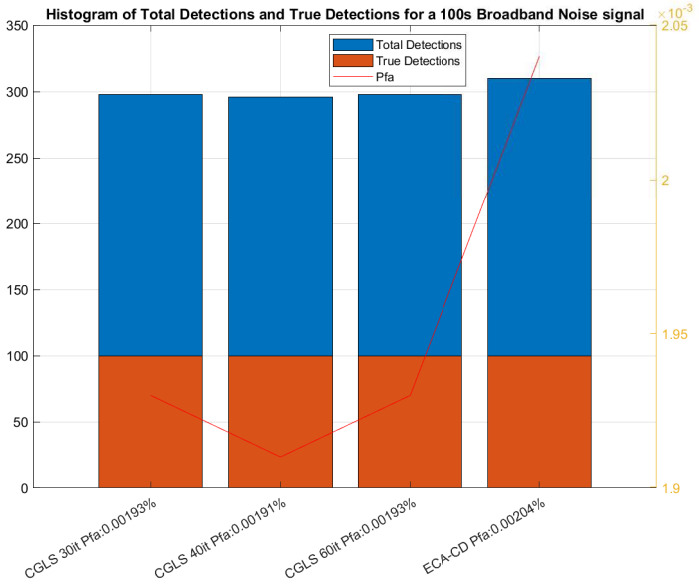

Figure 4.8: Histogram of the target detections and total detections for algorithms when used on a broadband noise signal.

The result in Figure 4.8 indicates that the P_{fa} increases for targets that are further away from the receiver. This has a more significant affect on CGLS where the P_{fa} increased to a value of 0.00193%, while the ECA-CD P_{fa} increased to a value of 0.00204%.

FM Signal Results and Discussion

The FM signal used in the simulations was recorded by an Armasuisse FM PR demonstrator.

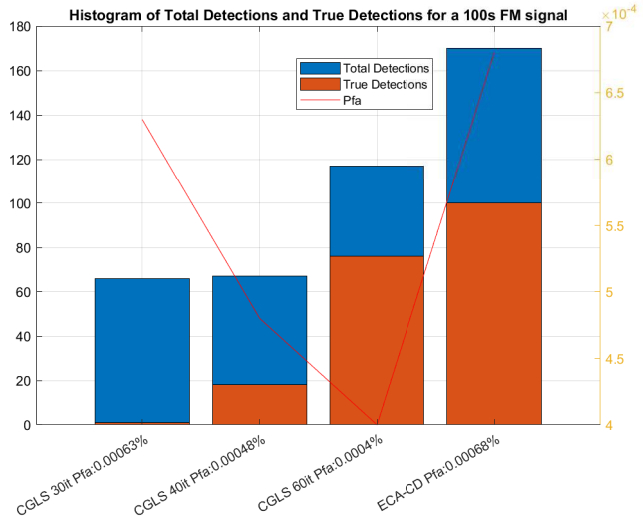

Figure 4.9: Histogram of the target detections and total detections for algorithms when used on a FM signal for the first target.

Figure 4.9 indicates that for a target closer to the receivers CGLS requires a high number of iterations for reliable target detection. The ECA-CD case has 100 out of 100 detections while the 60 iteration CGLS case has 78. The ECA-CD case has a slightly higher P_{fa} which is consistent with the previously established baseline. The P_d and P_{fa} of the 60 iteration CGLS case is lower for the FM signal than the simulated broadband noise.

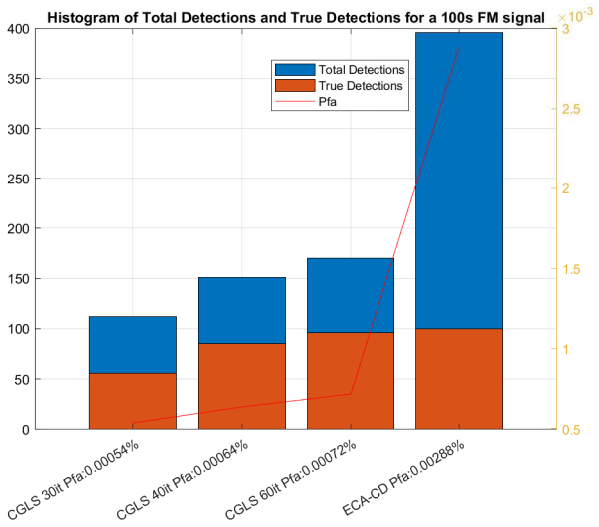

Figure 4.10: Histogram of the target detections and total detections for algorithms when used on a FM signal for the second target.

Figure 4.10 indicates that the probability of detection for the CGLS cases is significantly improved for targets further from the receivers, indicating that less iterations are required for effective cancellation when using CGLS. There is a relatively small increase in the P_{fa} for the CGLS cases, however the P_fa for the ECA-CD case more than doubles from a value of 0.00068% in Figure 4.9 to 0.00268% in Figure 4.10. Comparison to the broadband noise results in Figure 4.8 demonstrate that ECA-CD is negatively affected by the lower bandwidth of the FM signal and this becomes more prevalent for targets that are further away.

Processing Times

This system was used for simulation.

	Specs
Processor	Intel(R) Core(TM) i5-6200U CPU @ 2.30GHz 2.40 GHz
Installed RAM	8,00 GB (7,87 GB usable)
System type	64-bit operating system, x64-based processor

Table 4.3: Table of the specs of the computer used in processing.

Cancellation Algorithm	Processing Time
CGLS 30it	5.51 s
CGLS 40it	6.16 s
CGLS 60it	9.31 s
ECA-CD	4.08 s

Table 4.4: Table of the time for a single CPI to be processed in each suppression algorithm case.

Table 4.4 displays the processing times for a single CPI processed using each cancellation algorithm case. This demonstrates that ECA-CD is more computationally efficient than CGLS. This means ECA-CD may be useful for real time processing applications.

The results presented in this section demonstrate that ECA-CD is an effective DSI cancellation method for an FM passive radar. It is demonstrated to have a higher P_{fa} than CGLS when used on a broadband signal, even for lower numbers of iterations. When used on an FM signal it outperforms CGLS with 30 iterations, which is inadequate for the first simulated target. Compared to CGLS with 40 and 60 iterations ECA-CD has a higher P_{fa}, however, it requires less processing time and is more likely to detect the target. This indicates that ECA-CD is a trade-off of a higher P_d and lower processing time for a higher P_{fa} when compared to CGLS. Previous work has been done to optimise the CGLS algorithm for real-time processing [4]. With similar optimisation work it should be possible to achieve real-time processing with the more efficient ECA-CD algorithm. This trade-off is also acceptable when the targets of the radar are expected to have a high radar cross-section, increasing the target echo power level.

Chapter 5

OFDM Signals

This Chapter provides an overview of OFDM signals before describing the LTE signal and presenting the results of applying the equalisation technique used for DVB-T2 signals when processing LTE signals. The final section describes the specifics of the DVB-T2 signal and the pilot ambiguities.

OFDM signals are made up of closely spaced modulated carriers that have no ISI. The available spectrum is divided into what are known as sub-carriers, such that the peak of each sub-carrier is positioned at the peak of the previous as illustrated in Figure 5.1. Therefore, by definition, the sub-carriers are placed orthogonally from one another [76].

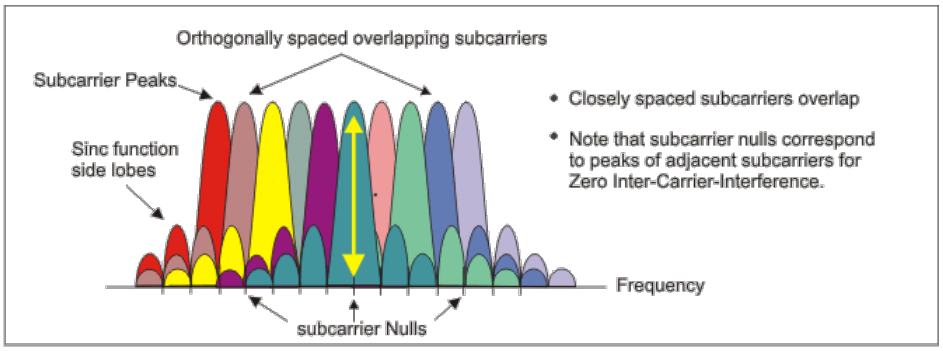

Figure 5.1: Illustration of the placement of sub-carriers in the FD of the OFDM signal.

By applying an IFFT to N sub-carriers, an OFDM symbol is created in the TD. A transmitted OFDM frame contains a number of symbols. A guard interval is placed at the start of every symbol to prevent ISI. This is achieved by copying the last portion of the symbol and adding it to the beginning of the symbol. This is known as a cyclic prefix. The frame structure of each OFDM technology differs and is defined by the relevant open standard.

OFDM signals have a high and consistent bandwidth when compared to analogue signals such as FM. This results in finer range resolutions in OFDM PR systems. By applying the demod-remod process a noise-free reference can be acquired to be used as a matched filter.

5.1 Ambiguity Equations

Guard Interval Ambiguities

Observing the structure of a symbol, during matched filtering the time interval at which the cyclic prefix convolves with its repeat at the end of the symbol is equivalent to τ_u. This is demonstrated in Figure 5.2 below.

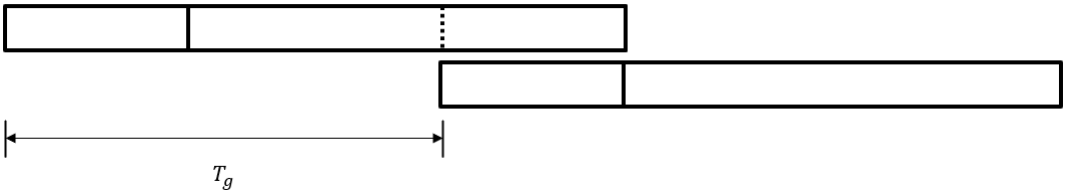

Figure 5.2: Figure demonstrating the cause guard ambiguity during matched filtering

This can be related to a delay range using the following equation:

$$R_g = T_u\, c \tag{5.1}$$

Where T_u is the integration period of a single symbol and c is the speed of light.

Range Ambiguities

There are symbols in both LTE and DVB-T2 that cause range ambiguities due to the repeated FD structure. These ambiguities repeat at integer multiples of R in the following equation:

$$R = \frac{c}{N\Delta f} \tag{5.2}$$

where N is number of symbols separating the consecutive equivalent symbols and Δf is the frequency spacing of the carriers.

5.1.1 Doppler Ambiguities

Doppler ambiguities are caused by symbols used to identify a frame and relay information. These symbols appear in the same This would be the SS in LTE and the Continual Pilots (CP) in DVB-T2. These ambiguities can be calculated as follows:

$$V_{rs} = \frac{1}{NT} \tag{5.3}$$

Where N is the number of symbols between the relevant symbols and T is the time over which the symbol is integrated.

5.1.2 inter-frame Ambiguities

The inter-frame ambiguities can be calculated using Equation 5.3 with T being equal to the time between frames. For higher integration times this calculation should be repeated for integer multiples of T based on the number of frames present in the CPI.

5.2 LTE

This section will introduce the reader to the physical description of the LTE signal. This is followed by a description of the ambiguities present in the AF of the signal. A thorough investigation into LTE as a PR IoO is presented for the remainder in the section.

The LTE signal used in this section is an Armasuisse European Aviation Network (EAN) recording from a PR receiver, therefore an EAN LTE signal or transmission is referred to for completeness. However the EAN signal follows the LTE standard and is not uniquely structured.

5.2.1 Signal Description

Resource Elements

The basic unit of an LTE signal is the Resource Element (RE) [77]. This unit is a single sub-carrier defined by its integration period, the portion of the signal on which information is encoded. A cyclic prefix (of standard or extended length) is then prepended to the integration period to form the complete RE. The integration interval [77] (T_u) of an RE is 66.67μs while the standard and extended guard intervals, T_g, are 4.7μs and 5.2μs respectively [77]. The inverse of the integration period implies that consecutive carriers in a given bandwidth will be separated by 15 KHz.

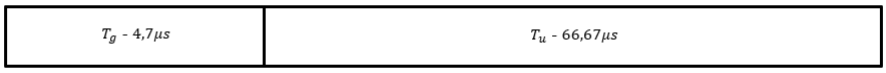

Figure 5.3: A RE with both the integration and guard interval which form a standard symbol duration

Resource Block

Combining these RE's in the FD will form a symbol. This is a set of 12 RE's occurring over a continuous bandwidth and a single guard and integration period. 7 of these symbols occurring consecutively form a single Resource Block (RB) as illustrated in Figure 5.4 [77]. By extension, in a given RB, there are 84 RE's. This implies a single RB will occupy a bandwidths of 180 KHz and take 0.5 ms to occur.

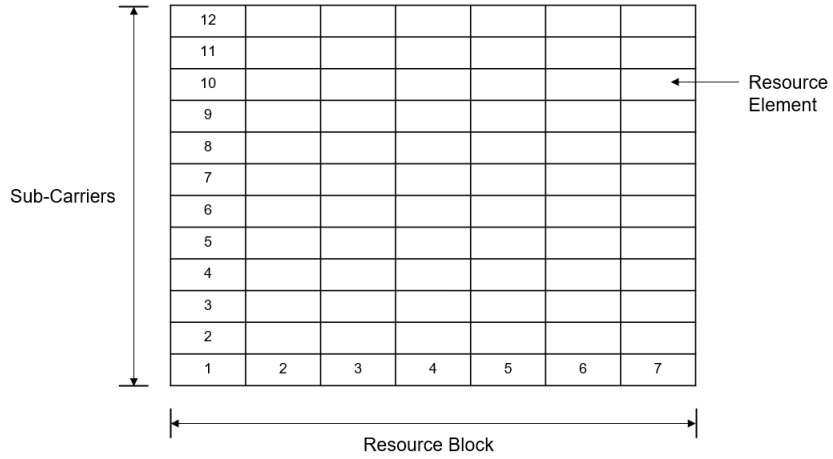

Figure 5.4: A RB with resource elements across multiple symbols in a single slot time ($0.5ms$)

Slot

The amount of time over which a RB occurs is the same as a RE 0.5 ms. The first RE in every RB has an extended guard interval therefore the RB occupies exactly 0.5 ms [77]. An important observation should be made at this point. The difference between a RB and slot is solely described by their bandwidths. Many RB's spread continuously across a bandwidth may be contained within a single slot time. Meaning, to find the number of RE's in a single slot time, the calculation would be the multiple of the number of RB's in a slot time and the number of RE's in a single RB(84).

Subframe

The sub-frame is the combination of two consecutive slots in time [77]. This logical division is important in terms of the distribution of signaling information and will come up in more detail in Section 5.2.2.

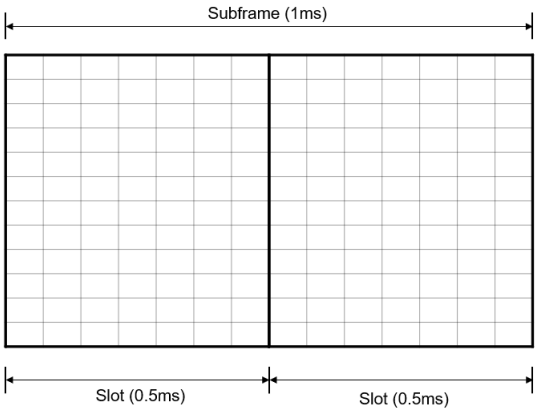

Figure 5.5: A Subframe (1 ms) that is comprised of two slots (0.5 ms)

Frame

A frame consists of 10 consecutive subframes (and therefore 20 slots) and is the largest unit in an EAN LTE transmission [77]. The number of RE's in a single frame, would be the multiple of the number of slots in a frame (20) and the number of RE's in a single slot. Furthermore, a frame time is 10 ms.

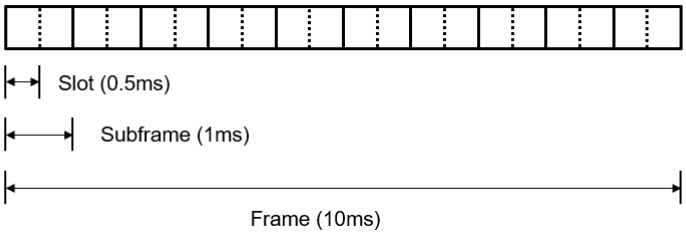

Figure 5.6: TD representation of frame with both subframes and slots

5.2.2 Signaling

Reference Signals

A portion of the RE's within any particular RB are allocated for signaling information. Of interest at this point is the RS. Multiple RE's within every single RB are modulated with RS codings. These allow for the cell search operations, downlink quality measurements and channel estimation. An example of how the RE's may be distributed in a RB is seen in Figure 5.7. The RS mapping to a particular RE index is repeated across every RB in a frame (in both time and frequency) for a particular downlink. i.e. the position of every RE (modulated with a RS) will be consistent and repeated across every RB. Note that the RS is encoded onto the RE. In the context of radar applications, this by implication, gives rise to two repeating points.

1. The RE pattern will repeat across RB's defined by the the cell ID, antenna port and symbol number. This does not necessarily guarantee that the complex modulation values modulated onto the RE will be the same.

2. The RS's complex modulation values will however repeat across frames defined by pseudo random sequences set out in the LTE standard.

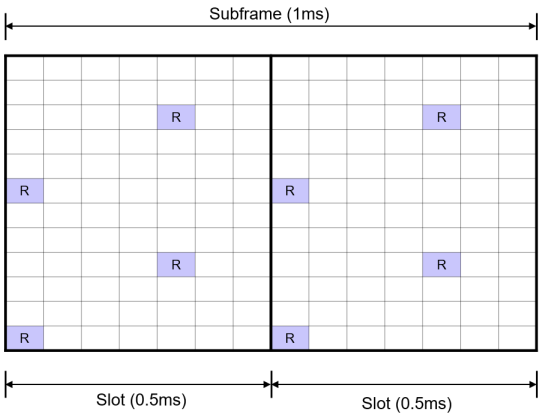

Figure 5.7: An example distribution (in time and frequency) of RE's that will be modulated with RS within a single subframe

Synchronisation Signals

The next signals to be discussed are the synchronisation signals. These are used to determine where a frame begins and ends. The Primary Synchronisation Symbol (PSS) is transmitted on the central 62 sub-carriers of the last symbol of time slots 0 and 10 [77]. The Secondary Synchronisation Symbol (SSS) is transmitted on the central 62 RE's of the second to last symbol of time slots 0 and 10. This means that both the PSS and SSS repeat twice in every frame. While the PSS is used for TD synchronisation the SSS is used to achieve radio frame synchronisation.

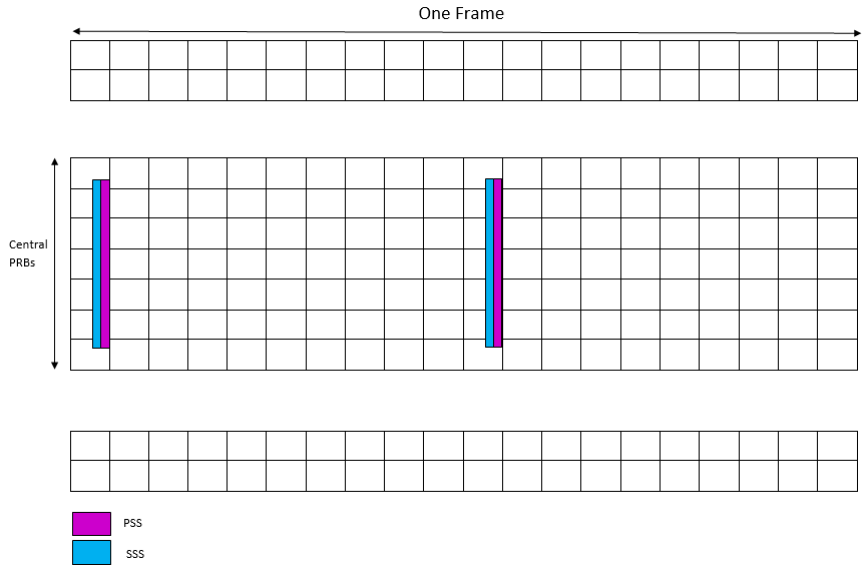

Figure 5.8: The synchronisation signals on the central 62 sub-carriers in slot 0 and 10 within a frame

5.2.3 Signal Summary

Signal Parameters

The Table below presents a final summary of the physical characteristics of the EAN LTE signal.

Parameter	Symbol	Value
Transmission Method	-	FDD
Carrier Frequency	2100 MHz	f_c
Integration Interval	66.67 μs	T_u
Guard Interval	4.7 μs	T_g
Symbol Duration	500 μs	T_s
Sub-carrier Spacing	15 kHz	Δf
Data Carriers per Symbol	7	-
Sub Carriers per Symbol	12	-
Bandwidth	15 MHz	-

Table 5.1: Table of the physical layer description of signal parameters for the EAN LTE signal

Repeating Signals

The Table below presents a summary of the repeating signals in the EAN LTE signal.

Signal Component	Time Repeat (s)	Frequency Repeat (KHz)
Reference Symbol	0.1	15
PSS	0.1	-
SSS	0.1	-

Table 5.2: Table of the time and frequency spacing between repeating signals in the EAN LTE signal

Frame View

The following diagram presents a visualisation of the frame including the distribution of all signaling information. Where light blue and purple RE's are the PSS and SSS, the red and grey RE's are allocated for RS in either one or the other colour and all other colours map to all other signalling information.

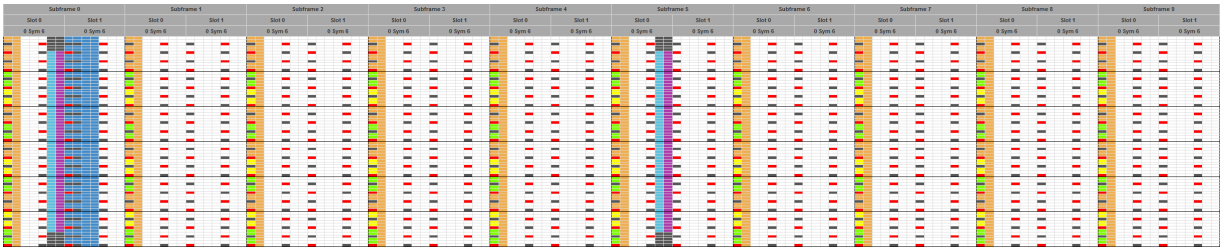

Figure 5.9: An example of the expected signaling information present in the central portion of the frame bandwidth [1]

5.2.4 Ambiguities

Guard Interval

The cyclic prefix is by definition the same as the end of the RE's integration period. This implies that when matched filtering a RE, ambiguities will occur. The maximum response will correspond to the perfect alignment between a RE and its matched filter. While the ambiguities will correspond to the matching of the cyclic prefixes and the signal itself.

Equation 5.1 can be used to relate this time to the corresponding range ambiguity. Using the signal parameters in Table 5.1 the ambiguity due to the guard interval is expected to occur at 19.987 km.

Expected Ambiguities Levels

Looking again at the signal structure, recall:

$$T_s = T_u + T_g \tag{5.4}$$

Where T_s is the symbol interval, T_u is the integration interval and T_g is the guard interval. The ratio between the the guard interval and the symbol interval is the same as the ratio of the power in the guard ambiguity with respect to the maximum power level (caused by a perfect symbol match). by

taking the log of this relationship the relative decibel difference between the previously mentioned peaks can be determined. Computing the relationship of the relative difference between the guard ambiguity and 19.987 km and the 0 range, 0 Doppler peak is as follows:

$$\Delta dB = 20log(\frac{T_g}{T_s}) = 20log(\frac{4.7}{71}) = -23.58dB$$

Downlink Reference Symbols

All signalling information will repeat in every frame (10 ms). These repeats over time cause Doppler ambiguities [78]. These are described with the equation below where this equation is an extension of the description of Doppler ambiguities in [78].

$$f = \frac{1}{T_{frame}} \tag{5.5}$$

Frequency Repetition - Range

Figure 5.9 demonstrates the repetition of the RS across the signal bandwidth for a given symbol period. These reference signals are separated by 6 RE's. Using the description of range ambiguities due to repeated FD structure in equation 5.2, the expected range ambiguities are at integer repetitions of 3.33 km.

Interframe ambiguities - Doppler

At this point the distinction made when discussing expected ambiguity levels becomes important. Looking at Figure 5.9 it may seem that the RS pattern repeats both within RB's, between slots and within the frame itself. This is not the case as the previously mentioned figure demonstrated the repeating RE which are encoded with differing RS's. For the repetition to consistently form ambiguities, the RS's would need to be the same across consecutive RE which they are not necessarily. This is the case as they the are generated by a pseudo random sequence and then assigned to an individual RE. After considering this point it should become apparent that the RS pattern will repeat between frames. Therefore using Equation 5.3 will produce the expected Doppler ambiguities. NT in this case becomes a frame time either with or without the guard interval (depending on the processing technique), 10 ms or 9.3 ms. Depending on the processing technique, the Doppler ambiguity would be at 200 Hz (guard included) or 214 Hz (guard not included).

Expected Ambiguities Levels

The ambiguities due to the RS's, PSS's and SSS's all occur at the level of a frame time. As such the Doppler ambiguities will occur at the same place. Therefirem the level of this particular ambiguity will be discussed jointly with the synchronisation signals.

5.2.5 Synchronisation Signals

Inter/Intraframe Ambiguities - Range

The synchronisation signal repeats every 10 ms and 5 ms when considering inter and intraframe transmissions. Using

$$R = cT \tag{5.6}$$

where c is is the speed of light and T is the time between repeated transmissions, the ambiguities in range are determined to occur at 3000 km and 1500 km. When considering the transmission power of LTE EAN transmission and ranges of interest, this range is determined to be inconsequential in terms of a practical radar system.

Interframe Ambiguities - Doppler

Equation 5.4 combined with the synchronisation signals repeated transmission every 10 ms implies that there will be Doppler ambiguities governed by Equation 5.3 repeated below.

$$V_{rs} = \frac{1}{NT}$$

As with Equation 5.4 N is the number of symbols between the synchronisation signals and T is the time over which the symbol is integrated. If the the guard interval is included in the radar processing integration time, the resulting value of T is 71 μs. Combining this with $N = 140$, the number in symbol periods between consecutive frame synchronisation signals, the resulting Doppler ambiguity will occur at 100 Hz. Additionally, if the guard interval is not included in the radar processing integration time, the value of T is altered to 66.67 μs. This results in Doppler ambiguities at 107 Hz.

Intraframe Ambiguities - Doppler

The above working can be reapplied within the frame itself. In this case, the presence of the synchronisation signals in the first and second half of the frame (as seen in Figure 5.9) must be recognised. The equivalent signal integration time between these two signals if the guard interval is assumed to be included in the processing is 5 ms, half a frame time. Using the formula above, the resulting Doppler ambiguity is 200 Hz. Alternatively, if the guard interval is not included during processing the resulting Doppler ambiguity is at 214 Hz.

Expected Ambiguities Levels

The ambiguity level calculation for the inter-frame Doppler ambiguity of the SS and RS can be calculated by dividing the number of RE's assigned to the SS's and RS's and dividing by the total number of RE's in a frame. The total number of RE's in a frame is 126000 while the number of RE's assigned to the SS's and RS signalling information is 6300. this puts the Doppler ambiguity at -26 dB. Although outside the scope of this section, it is important to note that all other signaling information if used will contribute additional power to the level of the ambiguity. This implies that the -26dB level is the minimum level of the ambiguity.

Ambiguities Summary

Ambiguity Source	Range	Doppler
Guard Interval	**20 km**	-
Reference Symbols	**3.33 km**	**200 Hz**
Intraframe Synchronisation Symbols	1500 km	**200 Hz**
Intraframe Synchronisation Symbols	3000 km	**100 Hz**

Table 5.3: A summary of the range and Doppler ambiguities caused by the signalling information contained within an EAN LTE signal

5.2.6 Complete Time Domain

The following analysis is conducted on a time-aligned EAN LTE signal. No further processing was conducted on the data. The following results are therefore a reference for all the ambiguities present in a standard EAN LTE signal.

Ambiguity Function

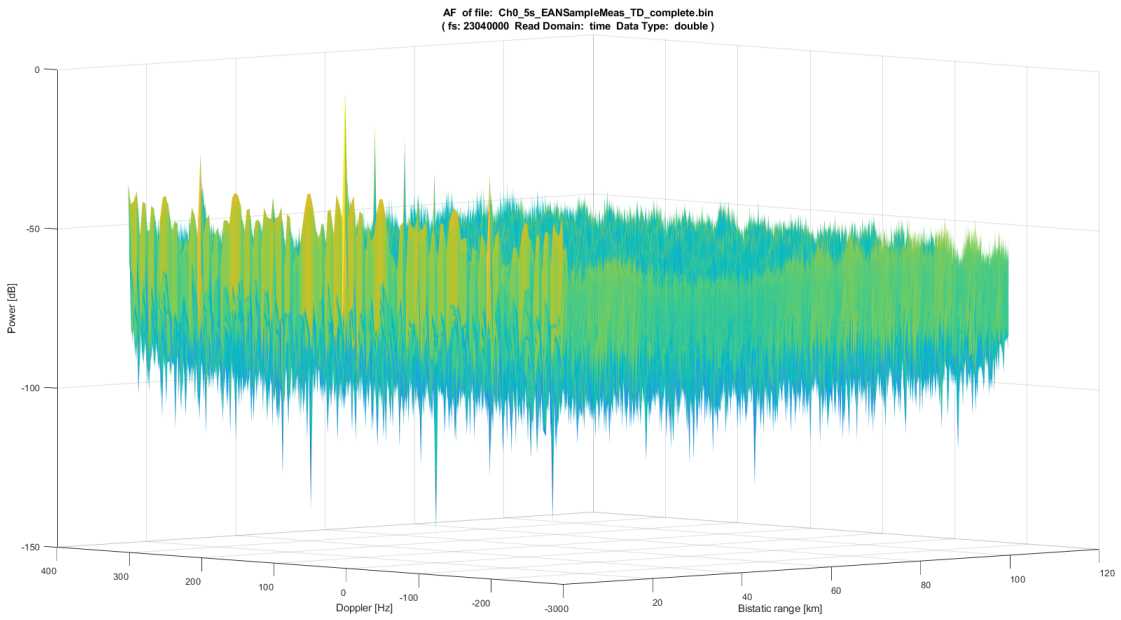

Figure 5.10: An ambiguity function of the time aligned EAN LTE signal with all signalling information present

Processing Parameters for Figure 5.10	
Surveillance	N/A
Reference	Time aligned TD signal
Processing type	FX
Processing Parameters	
Cancellation type	N/A
cancellation parameters	N/A
CPI samples	23.04e5(0.1s)

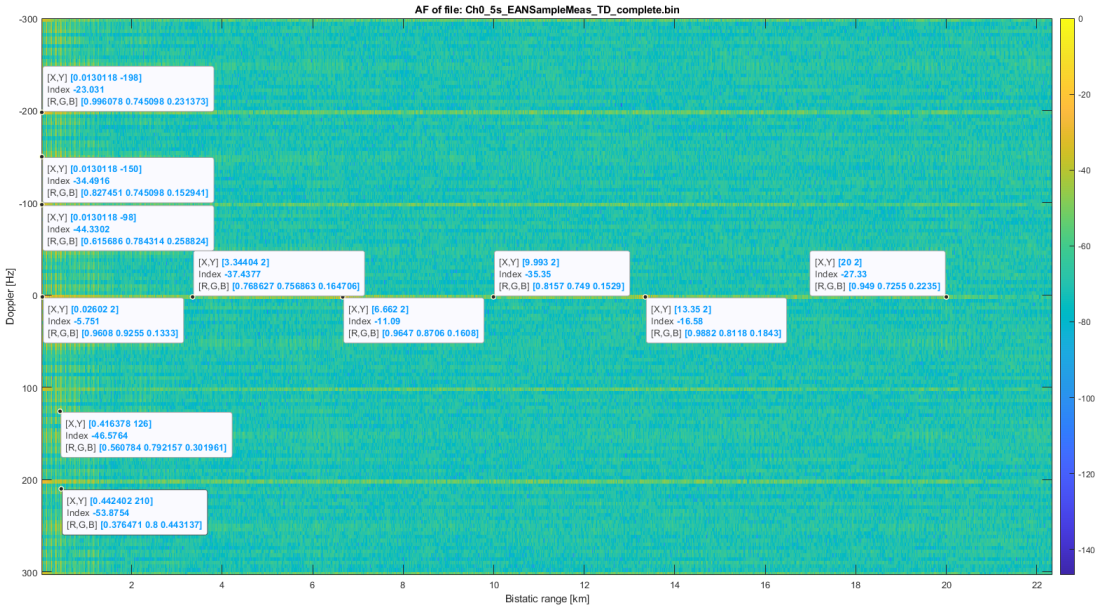

Figure 5.11: An AF of the time aligned EAN LTE signal with all signalling information present and notable ambiguities recorded

Processing Parameters for Figure 5.11	
Surveillance	N/A
Reference	Time aligned TD signal
Processing type	FX
Processing Parameters	N/A
Cancellation type	N/A
cancellation parameters	N/A
CPI samples	23.04e5 (0.1 s)

Observations and Discussion

As expected there are ambiguities in both range and Doppler as seen in Figure 5.10. Table 5.3 predicted their expected positions while Section 5.2.4 as a whole delves into the detail surrounding their sources.

Notable observations/characteristics from Figure 5.10 and 5.11 are as follows:

- The zero Doppler zero range index value is 0. This is due to the fact the the plots were normalised.
- The guard interval ambiguity as predicted by Section 5.2.4 occurs at a range of 19.99 km at a level of -27.33 dB.
- The RS ambiguities due to frequency repetition seen in Figure 5.9 as predicted by Section 5.2.4 occur at ranges that are multiples of 3.33 km.
- The Doppler ambiguities due to repeating time domain signals as predicted by Section 5.2.4 occur at Doppler frequencies that are multiples of 100 Hz.
- The Doppler ambiguity at 200 Hz is 21 dB higher than that at 100 Hz

5.2.7 Guard Interval skipped

The following analysis is conducted on a demod-remod EAN LTE signal with the guard interval removed. No further processing was conducted on the data. A notable implication of this processing the fact that the total time over which the signal is considered has been reduced as the guard interval is no longer included.

Ambiguity Function

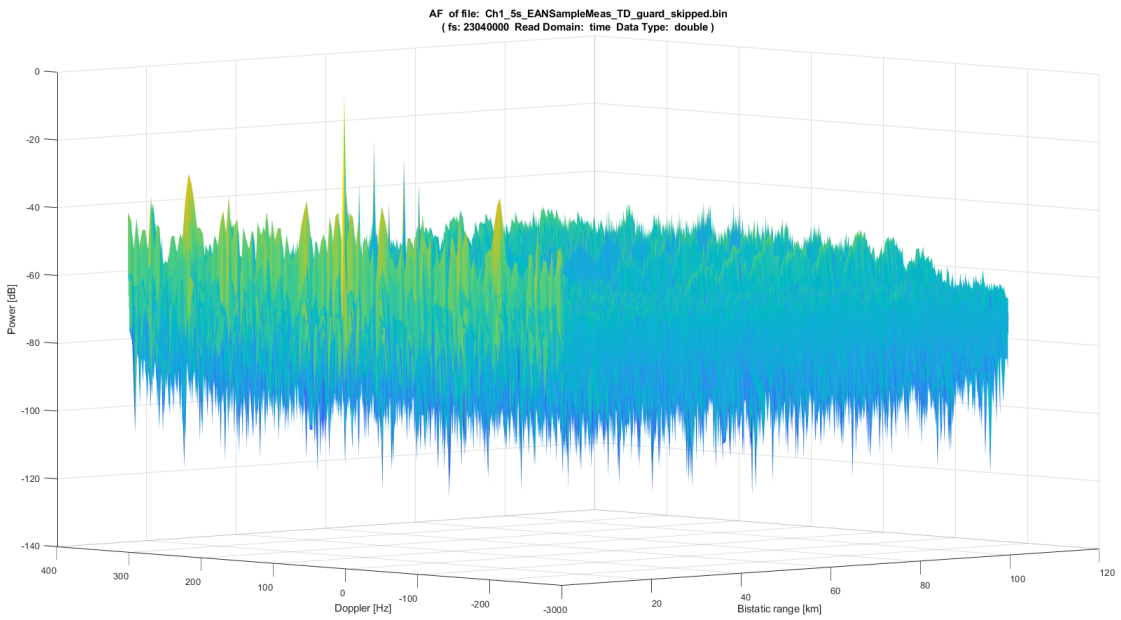

Figure 5.12: An AF of the time aligned EAN LTE signal with all signalling information present but the guard interval skipped

Processing Parameters for Figure 5.12	
Surveillance	N/A
Reference	Time aligned TD signal without guard interval
Processing type	FX
Processing Parameters	N/A
Cancellation type	N/A
cancellation parameters	N/A
CPI samples	23.04e5(0.1s)

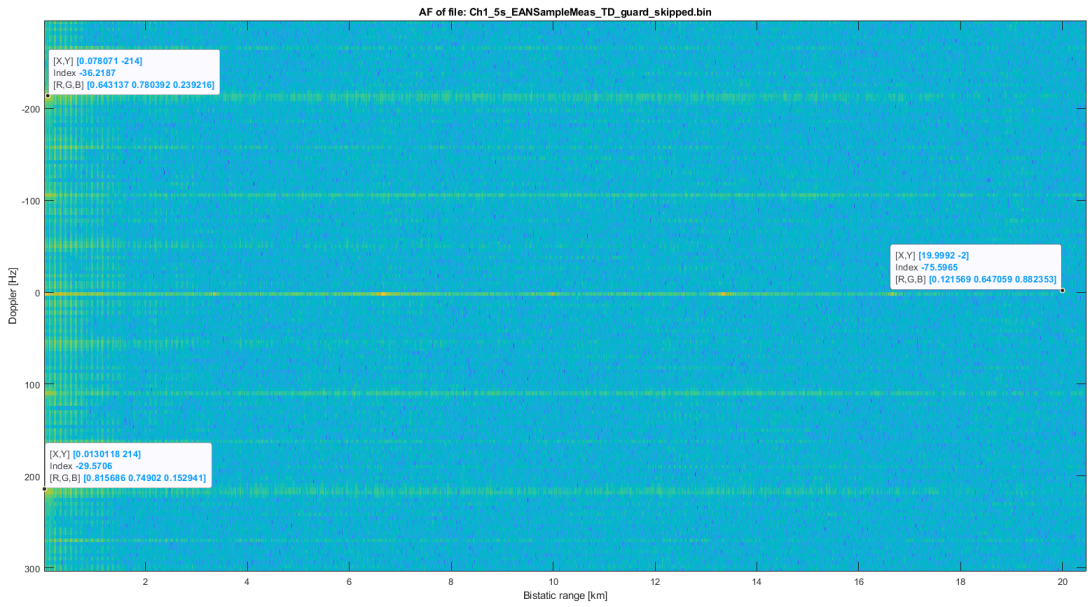

Figure 5.13: An AF of the time aligned EAN LTE signal with all signaling information present but guard interval removed. Additionally, notable ambiguities have been recorded

Processing Parameters for Figure 5.13	
Surveillance	N/A
Reference	Time aligned TD signal without guard interval
Processing type	FX
Processing Parameters	N/A
Cancellation type	N/A
cancellation parameters	N/A
CPI samples	23.04e5(0.1s)

Observations

Figure 5.12 and 5.13 displays the AF image of an EAN LTE signal with the guard interval removed. Notable observations include the following:

- The Doppler ambiguities now occur at 214 Hz instead of 200. This is due to the fact that the total time over which the signal has been considered is reduced. This was discussed in subsection 5.2.5.
- The guard interval ambiguity at 19.99 km observed in Figure 5.11 is now at -75.6 dB with respect to the figure maximum. This indicates that the ambiguity has been removed.

Reference Signals

The following analysis is conducted on only the symbols containing RS. All other symbols were 'nulled'. This was in an attempt to characterise the contribution of the RS's to the ambiguity function in Figure 5.10.

Spectrogram

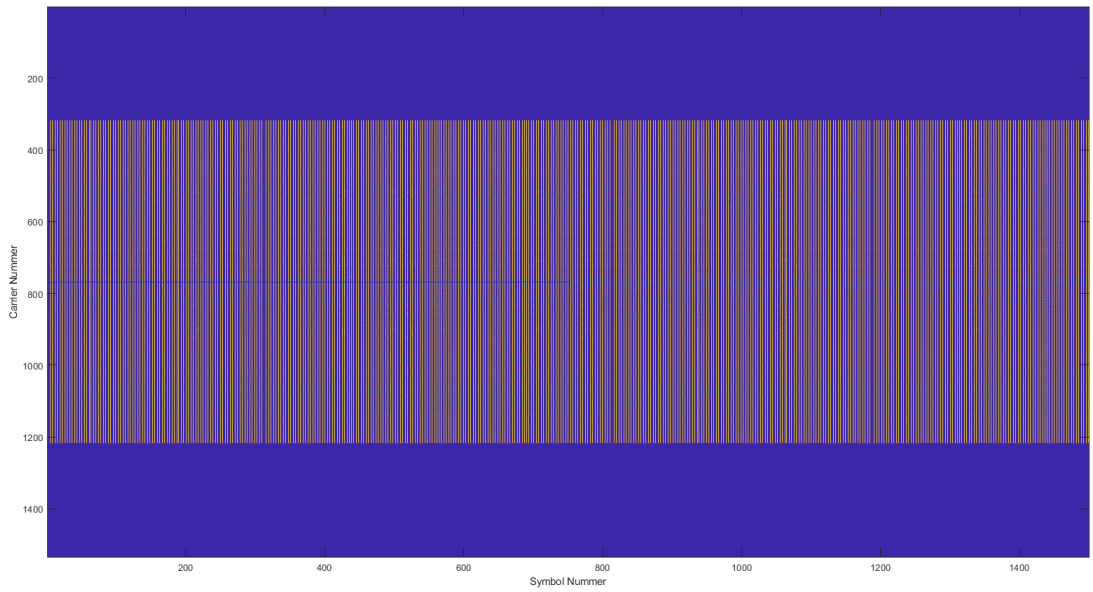

Figure 5.14: A spectrogram of all symbols nulled except those allocated to carry RS's

Ambiguity Function

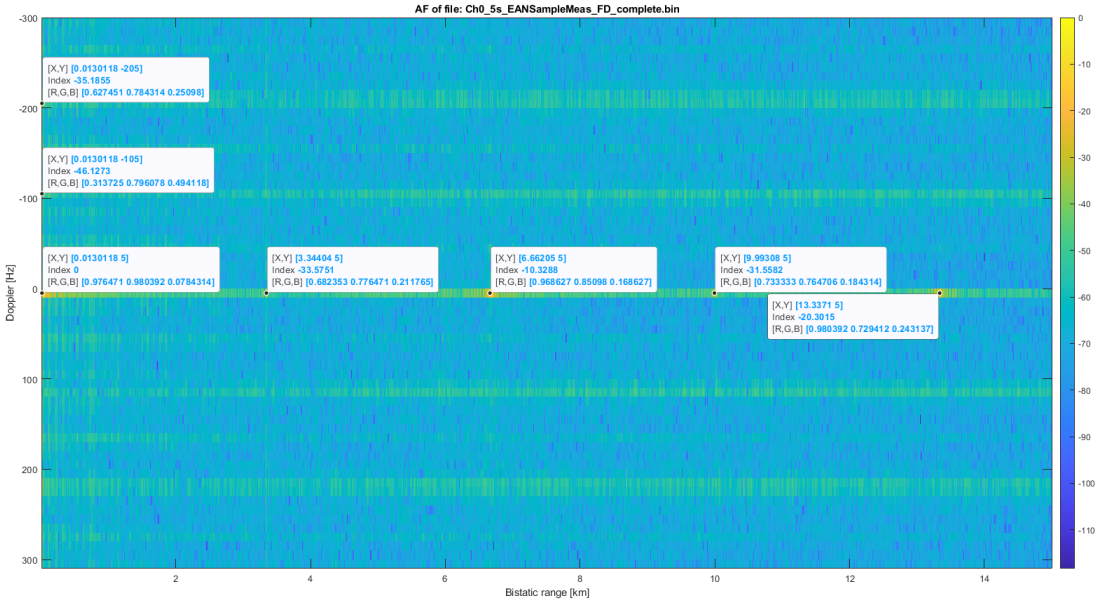

Figure 5.15: AF of all symbols nulled except those allocated to carry RS's

Processing Parameters for Figure 5.15	
Surveillance	N/A
Reference	Time aligned TD signal with all symbols nulled except those allocated to carry RS's
Processing type	FX
Processing Parameters	N/A
Cancellation type	N/A
cancellation parameters	N/A
CPI samples	23.04e5 (0.1 s)

Observations

Figure 5.15 displays the AF image of an EAN LTE signal containing only the RS in Figure 5.14. Notable observations from Figure 5.15 include the following:

- Range ambiguities as predicted in Section 5.2.4 occur at multiples of 3.33 km.
- Major Doppler ambiguities occur at multiples of 100 Hz as predicted by Section 5.2.4.

5.2.8 Synchronisation signals

Spectrogram

The following analysis is conducted on only the SS. All other symbols were nulled. This was in an attempt to characterise the contribution of the SS to the AF seen in Figure 5.10.

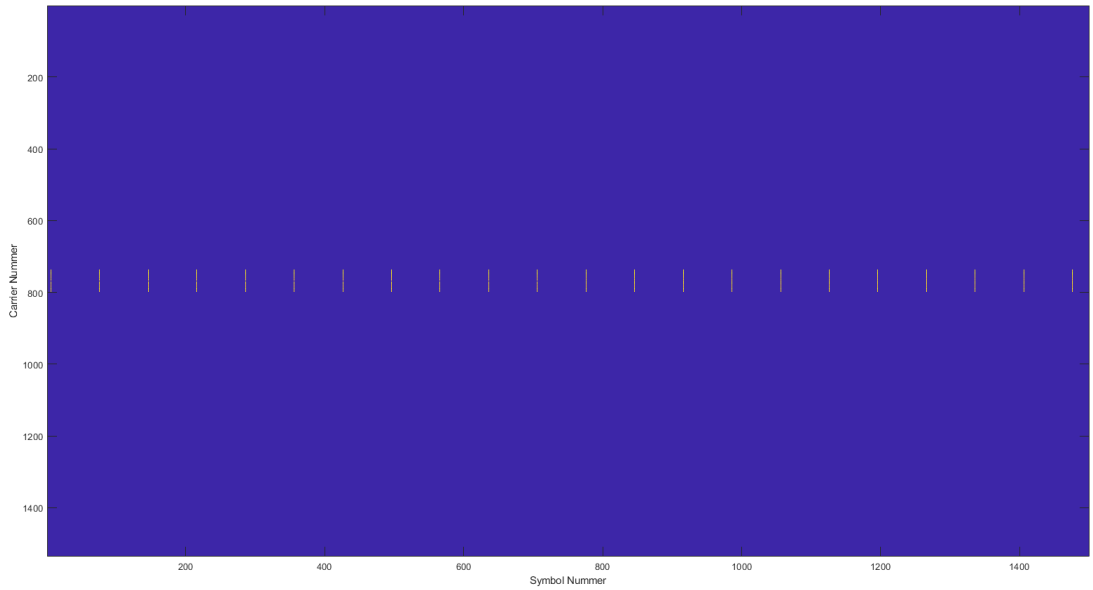

Figure 5.16: A spectrogram of the EAN LTE signal with RE nulled except the PSS and SSS

Ambiguity Function

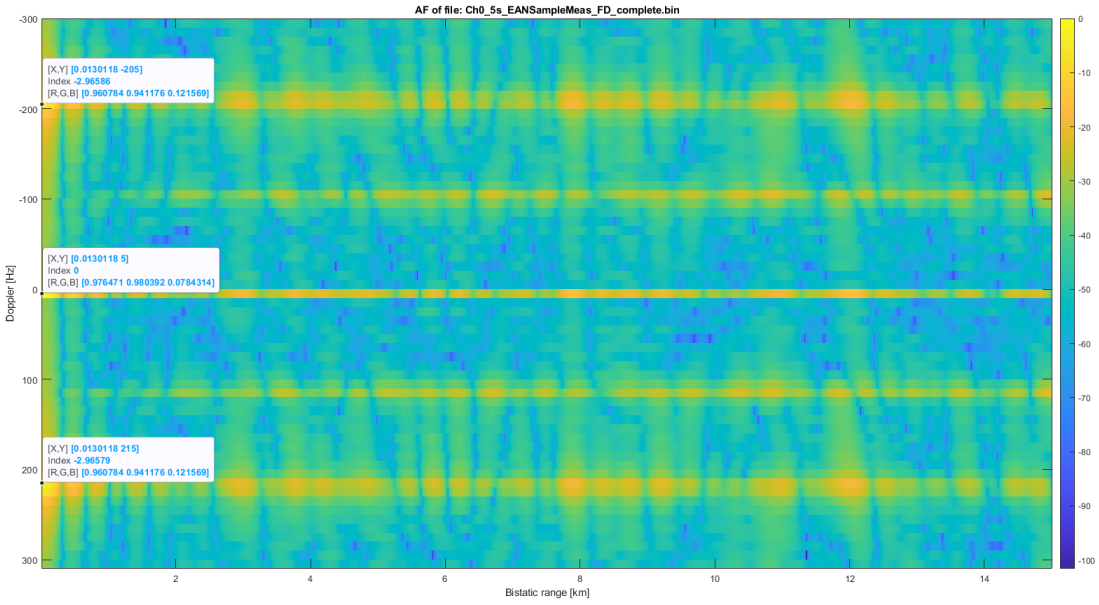

Figure 5.17: An AF of the EAN LTE signal with RE nulled except the PSS and SSS

Processing Parameters for Figure 5.17	
Surveillance	N/A
Reference	Time aligned TD signal with RE nulled except the PSS and SSS
Processing type	FX
Processing Parameters	N/A
Cancellation type	N/A
cancellation parameters	N/A
CPI samples	23.04e5 (0.1 s)

Observations

Figure 5.17 is the AF of an EAN LTE signal containing onli the SS seen in Figure 5.16. Notable include the following:

- As seen in Section 5.2.5 the SS signals cause Doppler ambiguities at 200 Hz.

5.2.9 Signal Equalisation

Reducing the power of the RS and SS in the reference channel reduces the ambiguities caused by the signals. The processing chain was modified to allow cancellation to occur using the time aligned reference and surveillance channels while using the modified reference for the ARD. The processing chain as seen in Figure 3.3 was used and is reiterated below for ease of reference.

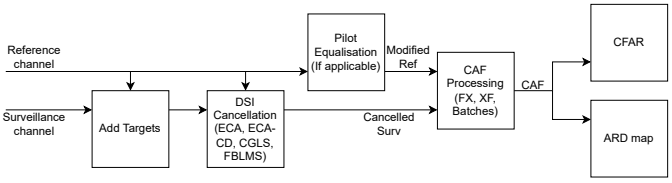

Figure 5.18: The complete processing chain with the pre-processing included.

The RS and SS equalisation was performed in the FD, therefore FD LTE signals were used as the input. In the LTE case, equalisation was performed by simply reducing the known carriers of the RS's and SS's. Figures 5.19 and 5.20 demonstrate how this processing affects the LTE signal structure.

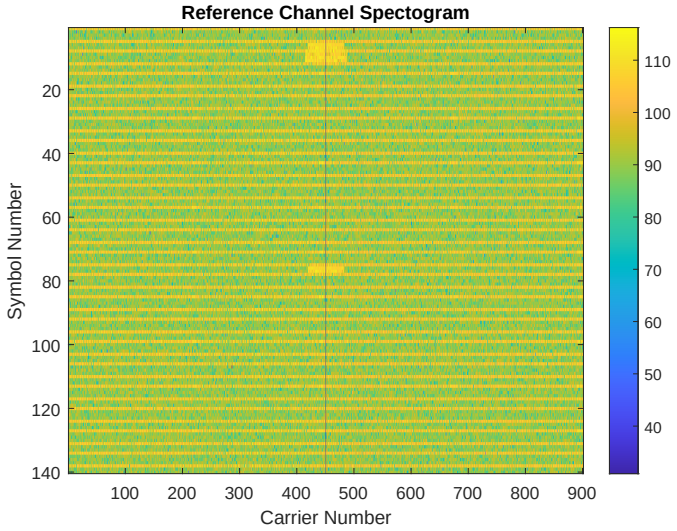

Figure 5.19: The reference channel spectrogram of LTE frame one.

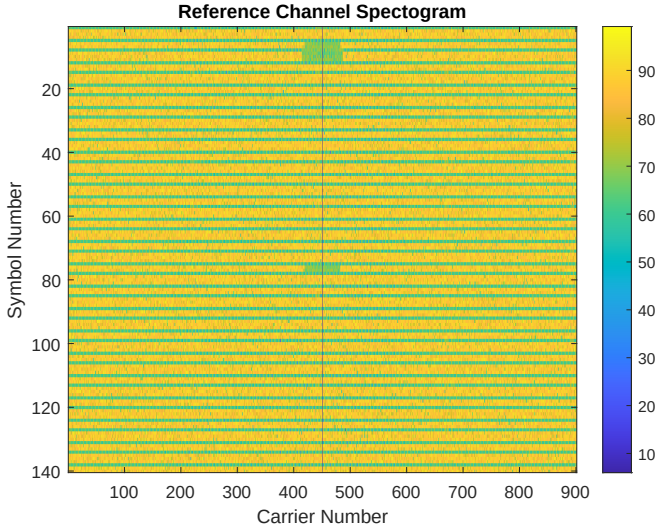

Figure 5.20: The reference channel spectrogram of a LTE frame one after the reference and SS carriers have been equalised using an equalisation factor of 0.007.

The equalisation factor used in Figure 5.20 was multiplied with the linear power values at carriers where RS's and SS's were present. The value of 0.007 was determined by trial and error as a clear power boosting value wasn't found. The output ARD was compared to the unequalised case where ambiguities were present and the case where the RS's and SS's are completely removed to find a balance between the two.

5.2.10 Simulated Targets

Simulated targets were added to the signal to determine if targets can be detected in an LTE signal using the processing chain.

Target	Target Range(km)	Target Doppler Shift(Hz)	Target SNR(dB)
Target 1	4.4	2200	-60
Target 2	7.6	-2500	-63
Target 3	12	4300	-68

Table 5.4: Table of the range, Doppler shift and power level of the simulated targets.

5.2.11 Simulation Results

For comparison the ARD map when only batches is applied is displayed in figure 5.21. The ARD maps in this section are for a single LTE frame of data. Therefore, the integration interval is 0.01 s.

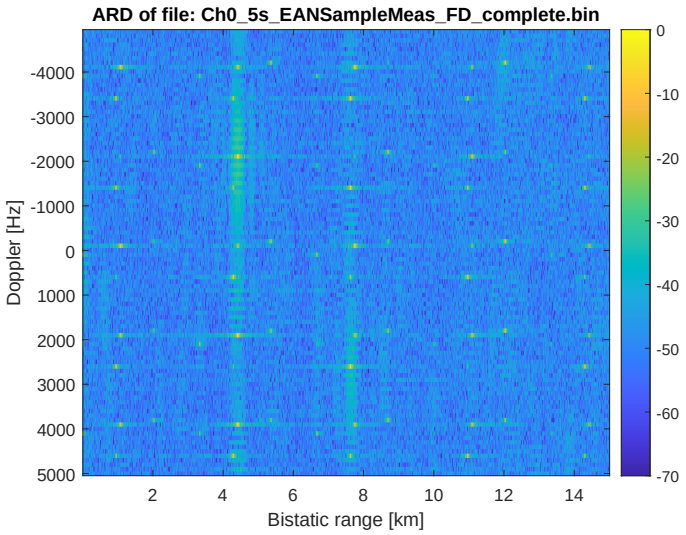

Figure 5.21: The ARD using Batches, no cancellation and no pre-processing.

Processing Parameters for Figure 5.21	
Surveillance	CH1 FD signal aligned to an LTE frame
Reference	CH0 FD signal aligned to an LTE frame
Processing type	Batches
Processing Parameters	nPulses=100
Cancellation type	None
cancellation parameters	N/A
Pre-processing type	None
Pre-processing Parameters	N/A
CPI samples	23.04e4 (0.01 s)

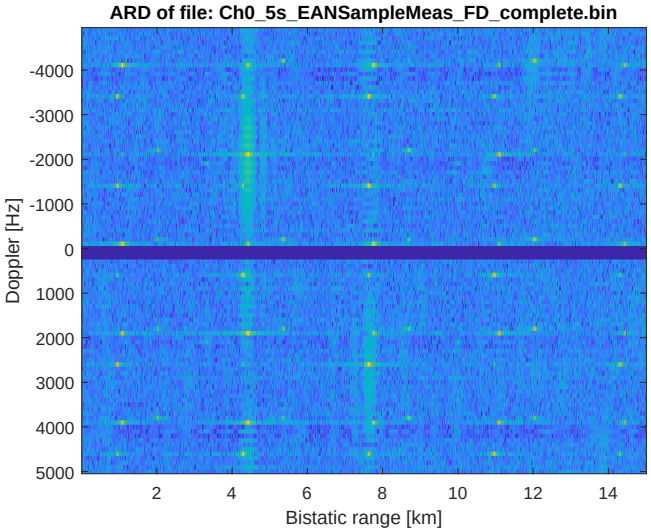

Figure 5.22: The ARD using ECA-CD, Batches and no pre-processing.

Processing Parameters for Figure 5.22	
Surveillance	CH1 FD signal aligned to an LTE framee
Reference	CH0 FD signal aligned to an LTE frame
Processing type	Batches
Processing Parameters	nPulses=100
Cancellation type	None
cancellation parameters	N/A
Pre-processing type	None
Pre-processing Parameters	N/A
CPI samples	23.04e4 (0.01 s)

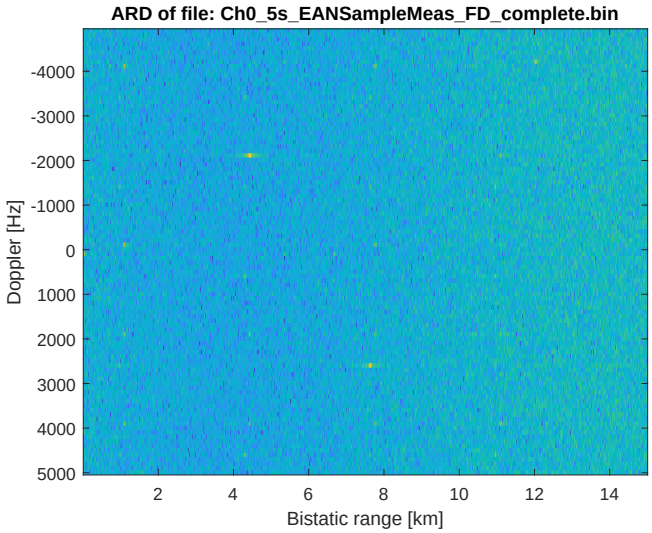

Figure 5.23: The ARD using ECA-CD, Batches and reducing the SS's using an equalisation factor of 0.007 in preprocessing.

Processing Parameters for Figure 5.23	
Surveillance	CH1 FD signal aligned to an LTE frame
Reference	CH0 FD signal aligned to an LTE frame
Processing type	Batches
Processing Parameters	nPulses=100
Cancellation type	ECA-CD
cancellation parameters	nPulses=100
Pre-processing type	Reduction
Pre-processing Parameters	RF=0.007
CPI samples	23.04e5 (0.1 s)

By comparing the peaks in the ARD in Figure 5.23 to Table 5.4 it can be seen that the three targets are present. The targets are positioned as defined in Section 5.2.10 This demonstrates that the processing chain can sufficiently cancel and reduce the effect of the LTE signal structure to allow for target detection in a transmitted LTE signal by making use of the equalisation processing technique.

5.3 DVBT2

DVB-T2 is an OFDM signal that is seeing increased use around the world [36]. PR systems that make use of DVB-T2 as well as it's predecessor DVB-T have been demonstrated various times [51, 79, 80, 81, 48].

5.3.1 Signal Structure

The smallest element of the DVB-T2 signal is the sub-carrier, or symbol, similar to the LTE RE. The data in each symbol is carried using Quadrature Amplitude Modulation (QAM). The structure of the DVB-T2 signal is standardised with the number of sub-carriers being dependent on the operating mode. Data symbols make up a T2, the number of which depends on the length of the symbols. When using 32K symbols (i.e. 32768 samples) then 60 symbols make up a T2 frame. Figure 5.24 below illustrates the TD structure of a T2 frame. Each T2 frame is 250 ms long and 255 T2 frames make up a super frame which is the third and highest abstracted level of the signal.

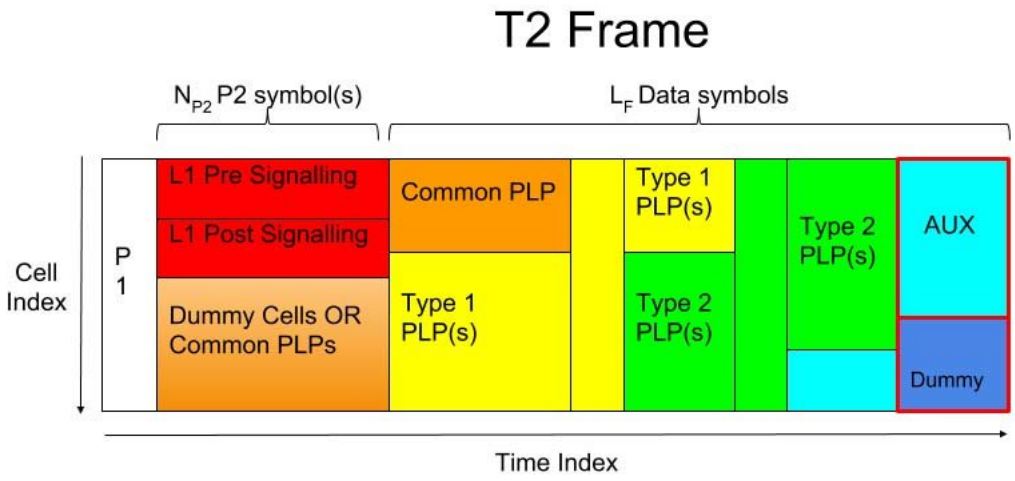

Figure 5.24: T2 frame structure without guard interval.

The P1 symbol is a 1K (1024 samples) symbol present at the beginning of every frame. It contains information about the FFT size of the other OFDM symbols in the frame. These can be 32K, 16K, 8K, 4K, 2K and 1K. It also contains information about whether Multiple Input Single Output (MISO) or Single Input Single Output (SISO) is being used. The P1 symbol is used to speed up the channel search and allows for timing and coarse frequency offset correction between the receiver and the transmitter.

The P2 symbols are split into Layer-1 (L1) signaling is split into L1-pre signaling and L1-post signaling and a dense pilot pattern. There are many more pilot tones present in a P2 symbol than there are in a data symbol. The number of pilot tones is dependent on the parameters given by P1. The L1 signaling allows for the demodulation of the DVB-T2 frame and the extraction of information. This includes the number of data symbols, the size of the constellation and the pilot pattern of the data symbols. Contained within the data symbols are data and pilots. The pilots are grouped into Physical Layer Pipes (PLP). The pilots can be divided into Scattered Pilots (SP) and CP. The SP are spread across the symbol and frequency bins. There are 8 pre-defined patterns using a Binary Phase Shift Keying (BPSK) mapping scheme defined by the standard [55]. The number of each PLP is in the L1 signaling. The remaining cells are not necessary for demodulation and are made of transmitter-specific streams or empty dummy cells.

5.3.2 Ambiguities

DVB-T2 pilots and guard interval cause ambiguities in the resulting ARD map due to being boosted to a higher power level than the data carriers. The AF is used to display the ambiguities caused by the pilots. Figure 5.25 is the AF of a single frame of the DVB-T2 signal.

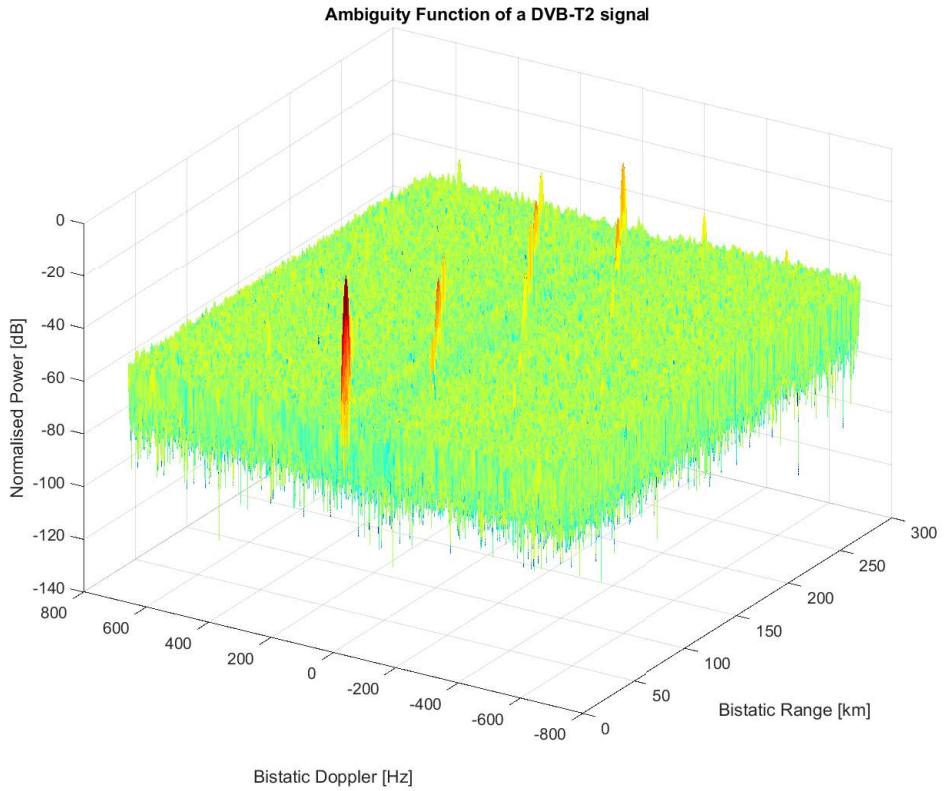

Figure 5.25: AF of the DVB-T2 signal.

The signal used has symbols with a FFT size of 32k, resulting in guard and interframe ambiguities being beyond the expected detection range of a DVB-T2 PR system.

Guard Interval Ambiguities

These ambiguities occur due to the repitition of the cyclic prefix both within a symbol and between symbols. The guard ambiguity is a function of the time interval of a symbol T_u. For 32K with a 2K symbol T_u is 3.584 ms the guard interval ambiguities appear at more than 1000 km, well beyond the expected detection range of PR systems [3]. For symbols with a smaller FFT size (2K,4K) these may become relevant as they appear closer.

Inter-symbol ambiguities

Inter-symbol ambiguities occur due to symbols correlating between different symbols within the integration time. These occur at a delay of 3.584 ms or more for a 32K symbol. As a result these also appear beyond the expected detection range of PR systems, however for 2K and 4K symbols these are relevant.

Intra-symbol ambiguities

The intra-symbol ambiguities are caused by the repeated pilots with a single symbol. These can be calculated using Equation 5.2 for the range ambiguities caused by the SP's and Equation 5.3 for the Doppler ambiguities caused by the CP's. The equalisation of the pilots removes these as shown by [81] and results in a CAF as seen in Figure 6.3 in Section 6.

5.3.3 Ambiguity Removal

The ambiguities can be mitigated by equalising the pilots during the remodulation process as shown in [47]. There are various ambiguity regions that must be considered as discussed by Paine [3] using processes described by Gao [39] and Harms [41].

Intra-symbol Ambiguities

One method of removing Intra-symbol Ambiguity is to blank the pilots (setting their value to zero) as proposed by O'Hagan et al. [47] and demonstrated by Kovalev et al. [46], however the resulting inverted pulse train leads to ambiguities in the same positions in the ARD map [3]. Therefore, a normalisation or equalisation approach is taken, bringing the pilot levels down to the level of the data carriers using an equalisation factor of $(\frac{4}{7})^2$. This results in a decrease in integration gain of about 0.44 dB [3].

Inter-symbol Ambiguities

The inter-symbol ambiguities cause by pilots repeated over different symbols can be removed in much the same way. Generally, these can be ignored as they will lie beyond the range of the radar. A solution to these ambiguities demonstrated by Gao et al. [39] is to blank the pilots for the inter-symbol ambiguities and equalise the pilots for the intra-symbol. The ambiguity regions are calculated in parallel and the ARD map is formed by stitching the results together.

Guard Interval Ambiguities

The guard interval ambiguities are caused by the cyclic nature of the guard interval in each symbol. These only occur over multiple symbols as the guard interval repeats. By blanking the guard interval in the remodulation step these ambiguities can be removed [44, 41, 39]. This causes a loss of integration gain in proportion to the guard interval length.

Chapter 6

Results and Discussion

6.1 Overview

6.2 Summary

In this section the method of target simulation is first discussed. This is followed by the resulting ARD maps produced when applying the processing chain to each of the discussed signals. The results indicate that the processing chain is effective for FM, DVB-T2 and LTE PR signals. Note that no real-time optimisation or parallelisation was implemented.

	Specs
Processor	Intel(R) Core(TM) i5-9500 CPU @ 3.00 GHz
Installed RAM	16 GB RAM
System type	64-bit operating system, x64-based processor

Table 6.1: Table of the specs of the computer used in the processing.

6.3 Target Simulation

To simulate targets, a copy of the reference channel is made with reduced power, shifted doppler and a time delay. This copy is then added to the surveillance channel and the result is the output of the function. This is achieved using the method described in Chapter 3. The targets were simulated and positioned as per Table 6.2.

Target	Target Range (km)	Target Velocity (m/s)	Target SNR (dB)
Target 1	34	-300	-60
Target 2	22	250	-63
Target 3	13	100	-68

Table 6.2: Table of the range, Doppler shift and power level of the targets.

6.4 FM Results

The input FM signal is a normalised recording from a FM PR demonstrator.

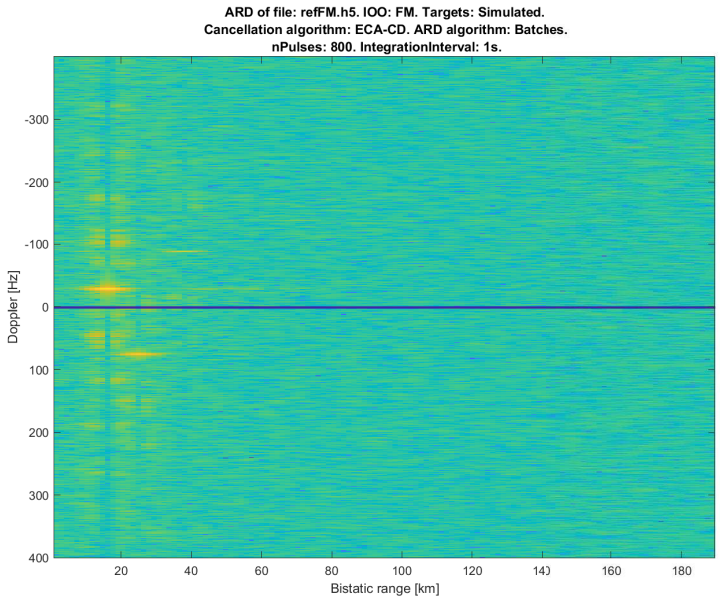

Figure 6.1: ARD of the FM signal, simulated targets, using ECA-CD and Batches.

Processing Parameters for Figure 6.1	
Signal	txWaveformNormalised.h5
Processing type	Batches
Processing Parameters	nPulses=800
Cancellation type	ECA-CD
cancellation parameters	nPulses=800
CPI samples	240e3(1s)

Notable observations from this plot are:

- By visual inspection all three targets appear in the ARD
- Targets closer to the origin appear to cause significant striations and targets further from the origin are clearer and easier to resolve.

To determine if the processing chain has simulated and detected the target echoes at the correct locations and velocities, Figure 6.2 is the same plot with datatips on the peaks of apparent detections:

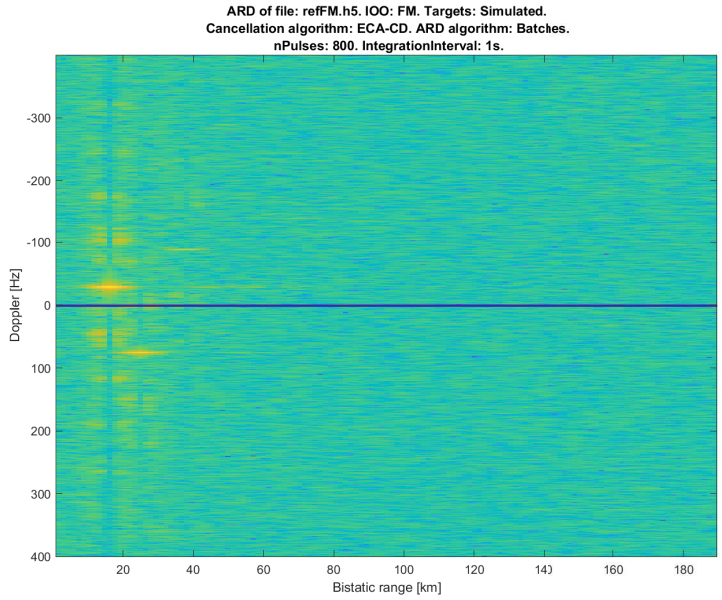

Figure 6.2: ARD of the FM signal, simulated targets with datatips, using ECA-CD and Batches.

Using the X and Y values of the datatips, the bistatic range to the target and the Doppler shift can be observed.

6.4.1 Discussion

By referring to Table 6.2 it appears that the target echoes are correctly located. The results indicate that the processing chain can effectively detect targets in an FM signal. The coarse range resolution results in poor bistatic range estimation of the target, however, the fine Doppler resolution allows for accurate velocities to be extracted. Due to the striation at relatively close ranges, the FM signal is useful for long-range detection in a generalised PR system. For the 1s CPI the processing chain was relatively fast, taking 1.608s to process the data and the ECA-CD process taking 1.6s.

6.5 DVB-T2 Results

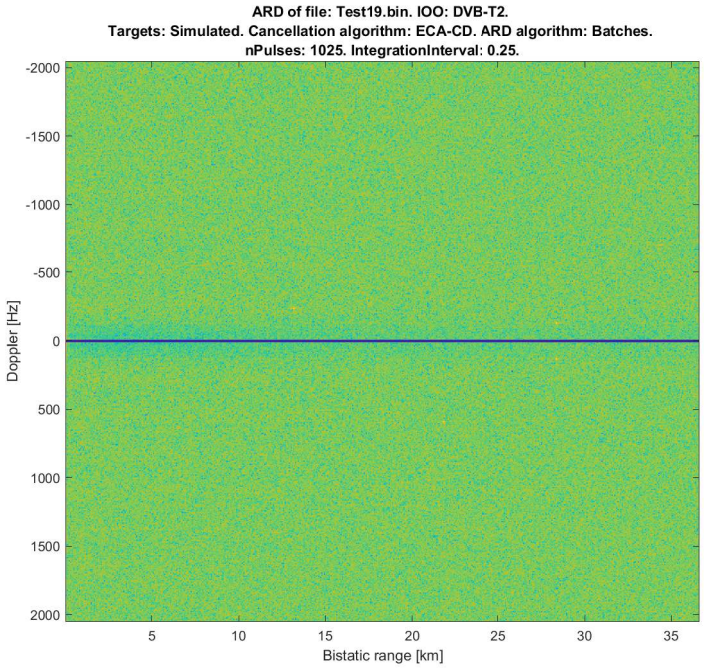

Figure 6.3: ARD of DVB-T2 signal, simulated targets, using ECA-CD and Batches.

Processing Parameters for Figure 6.3	
Signal	CH0 FD signal aligned to an LTE frame
Processing type	Batches
Processing Parameters	nPulses=1025
Cancellation type	ECA-CD
cancellation parameters	nPulses=1025
Pre-processing type	Equalization
Pre-processing Parameters	Equalisation factor=$(\frac{4}{7})^2$
CPI samples	228575(0.25s)

The fine range and Doppler resolutions of the DVB-T2 signal make the target echo peaks difficult to see, however several observations can be made:

- All targets are present.
- For the simulated distance there does not appear to be artifacts or striations caused by targets closer to the origin.
- The guard interval creates ambiguities at a certain range.

For ease of visualisation and to determine if the targets are correctly located, Figure 6.4 is the same plot with datatips on the peaks of the target echoes.

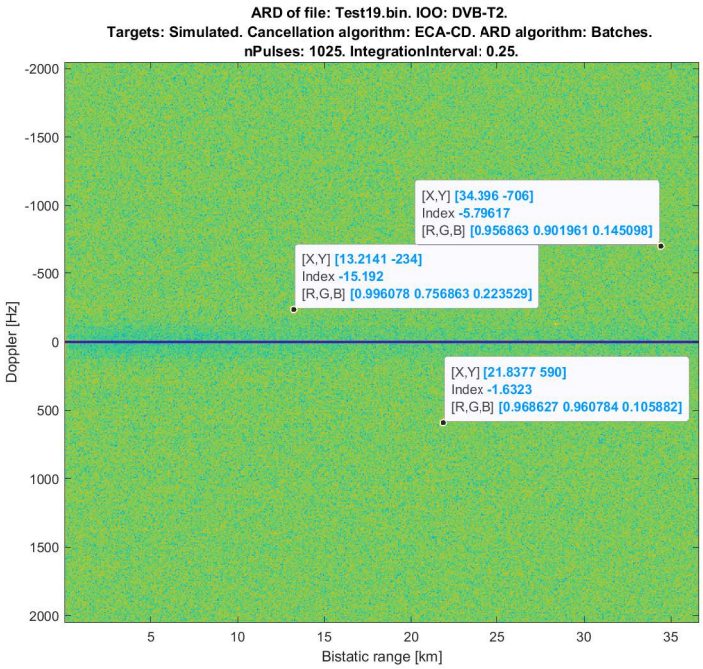

Figure 6.4: ARD of the DVB-T2 signal, simulated targets with datatips, using ECA-CD2 and Batches processing.

6.5.1 Discussion

By referring to Table 6.2 it can be observed that the target echoes are very close to the expected values. The fine range and Doppler resolutions allow for effective extraction of range and velocity of the target. Targets can also be detected at relatively long ranges. The processing time for DVB-T2 was 23.127s, relative to the CPI this was the slowest result. This is caused by a high sampling rate and a comparatively low number of ECA-CD pulses resulting in larger arrays to be processed. The CPI and ECA-CD can be adjusted in the future for optimisation.

6.6 LTE Results

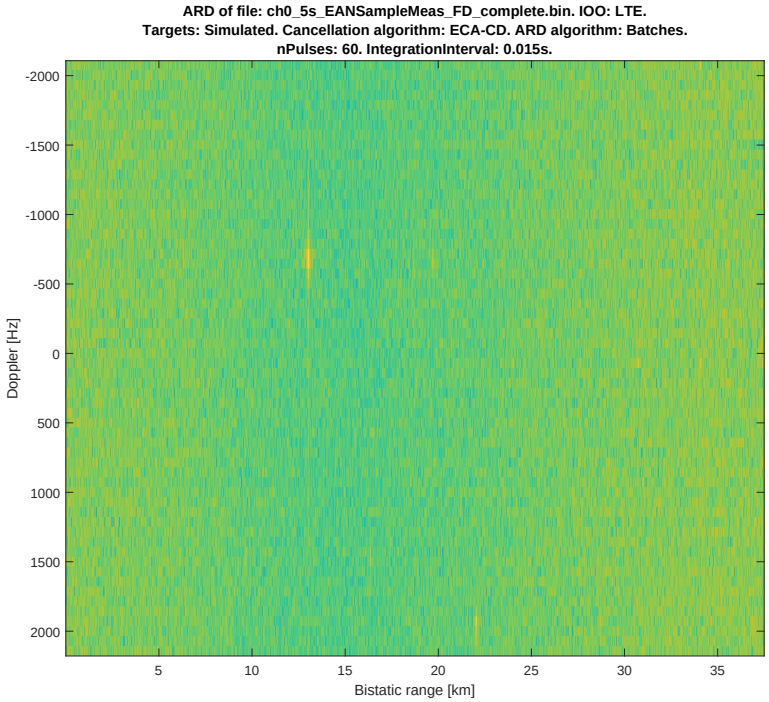

Figure 6.5: ARD of the LTE signal, simulated targets, using ECA-CD and Batches processing.

Processing Parameters for Figure 6.5	
Signal	CH0_EANSampleMeas_FD_Complete.bin
Processing Parameters	nPulses=50
Cancellation type	ECA-CD
cancellation parameters	nPulses=50
Pre-processing type	Equalization
Pre-processing Parameters	Equalisation factor=0.007
CPI samples	34.56e4 (0.015 s)

By inspection:

- All three targets are present.
- The furthest target is close to being outside of the Doppler range of the ARD.

The same plot is displayed in Figure 6.6 with Datatips placed on the peaks of the target echoes.

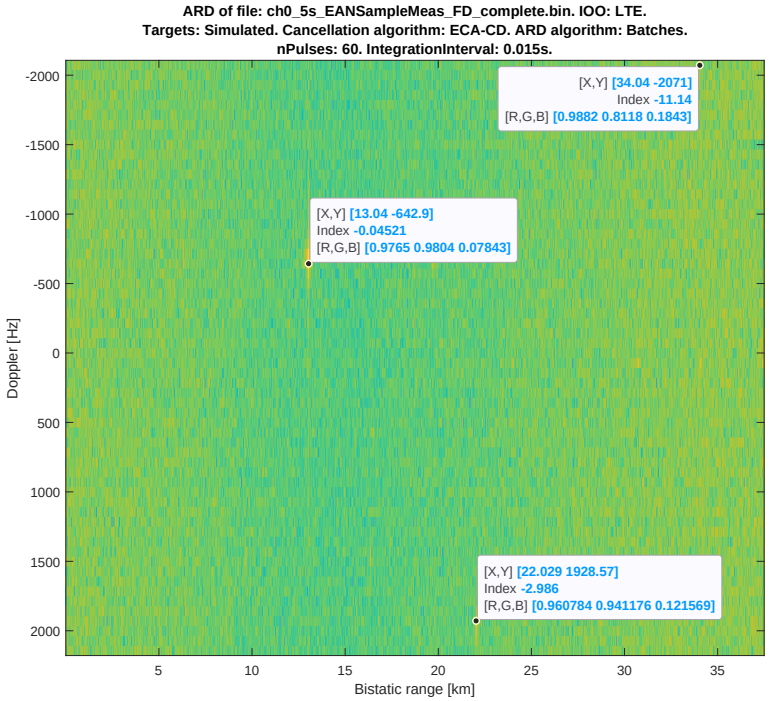

Figure 6.6: ARD of the LTE signal, simulated targets with datatips, using ECA-CD and Batches processing.

In reference to Table 6.2 it can be observed that:

- The target echoes are close to their expected positions.
- With the exception of the second target which is more than 100 Hz off the expected Doppler shift.

6.6.1 Discussion

The LTE signal has a relatively coarse Doppler resolution of due to the low integration interval. The Doppler resolution is $\frac{1}{0.015} \approx 67\,\text{Hz}$. Therefore he second target is about two Doppler bins off. For the 0.015s CPI the processing chain took 0.19s to process the data with the ECA-CD process taking 0.17s. Considering the high sampling rate necessary for LTE the processing chain works efficiently for processing LTE signals.

6.7 Final Observations

The proposed algorithm allows for target detection in FM, DVB-T2 and LTE signals. The results demonstrate that for an approach using ECA-CD and Batches, a number of different illuminators can be exploited for operational benefit. The FD approach used produced a high performance processing chain that works efficiently on both FM and OFDM signals. In the results, the maximum bistatic range and max/min Doppler displayed in the ARD maps of each signal type differ significantly. This means that while the processing chain is effective on all the signal types discussed, a system exploiting more than one signal type concurrently may need to use each for a different purpose. For example, a system exploiting both FM and DVB-T2 for scanning for aircraft with the purpose of classification and tracking would make the best use of the FM PR for long-range detection and the DVB-T2 PR for classification and tracking as a target moves closer. In Table 6.3 the proposed processing chain is demonstrated to be efficient without real-time optimisation and no parallelisation.

Signal	CPI	ECA-CD Compute Time	Batches Compute Time	Total Compute Time	Relative Time
FM	1s	1.6s	0.008s	1.608s	1.6
DVB-T2	0.25s	23s	0.127s	23.127s	92.5
LTE	0.015s	0.17s	0.019s	0.19s	12.6

Table 6.3: Table of the algorithm computation times for each signal structure on the hardware specs outlined in Table 6.1.

The Relative Time in Table 6.3 can be viewed as the time taken, in seconds, to process a 1s signal of the given signal structure. The table demonstrates clearly that when processing high bandwidth signals the relative processing time is significantly increased. The relative time results of 92.5 and 12.6 for DVB-T2 and LTE respectively seem to contradict this, however these results demonstrate how the number of pulses selected for ECA-CD and the number of samples in the CPI, affects the efficiency of the algorithm. The processing time comparison in Section 4.1.3 showed that ECA-CD was significantly more computationally efficient than CGLS and when considering the real-time processing chain demonstrated by Tong [4], real-time optimisation seems promising with these results.

Chapter 7

Conclusions and Future Work

The objective of this dissertation was to demonstrate a generalised processing chain for both analogue and digital signals. This allowed for a PR system making use of different IoO infrastructures to simplify deployment and maintenance of the code base. The focus of the work was to demonstrate that a generalised processing chain is possible and practical, therefore it was necessary to find DSI cancellation and ARD making algorithms that can be used for both analogue and digital signals. The algorithms at both processing stages were compared when used to process the FM, LTE and DVB-T2 signals to determine the most effective choice for the generalised processing chain.

To facilitate this investigation, a processing chain was designed where the DSI cancellation and ARD algorithms are interchangeable. In this state the processing chain is bulky, however it facilitates the comparison of the DSI cancellation algorithms with one another and the ARD algorithms with one another, as well as the different combinations of algorithms where FFTs are used to allow TD inputs to FD algorithms and IFFTs are used to allow FD inputs to TD algorithms.

7.1 Conclusions

7.1.1 FM FD processing

It is well established that TD algorithms can achieve real-time performance on low bandwidth signals, such as FM signals, however, due to the inherent FD nature of digital signals, an FD approach was required. Therefore, it is necessary to demonstrate that FM signals can be processed efficiently and effectively using not only TD approaches such as CGLS, but also FD approaches such as ECA-CD. An initial comparison was done using real world data with real targets to determine similarity by inspection of the ARD maps generated by the processing chain using both DSI cancellation algorithms. This comparison demonstrated that ECA-CD is a functional DSI cancellation method for FM signals.

An empirical demonstration, using the probability of false alarm (P_{fa}), target detections and processing time of CGLS using different numbers of iterations and ECA-CD were compared when applied to FM signals. These performance metrics were drawn from the CFAR output in each case.

Cancellation algorithm	Target 1 P_{fa}	Target 2 P_{fa}	Target 1 Detections	Target 2 Detections	Processing time
CGLS 30it	0.00063%	0.00054%	3	60	
CGLS 40it	0.00048%	0.00064%	18	80	
CGLS 60it	0.004%	0.00072%	76	90	
ECA-CD	0.00068%	0.00268%	100	100	

Table 7.1: Table of the results when ECA-CD is applied to an FM signal. 7.1.

ECA-CD outperformed CGLS in target detections for both targets. The P_{fa} for the first, closer targetm was similar. For the second target the P_{fa} for ECA-CD was significantly higher than when using CGLS. The detections and The P_{fa} indicate that CGLS performs better at long range while ECA-CD performs well at shorter ranges. In terms of processing time, it was demonstrated that ECA-CD is significantly faster than CGLS. With acceptable performance and a significantly lower processing time, these results demonstrated that ECA-CD is an effective DSI cancellation algorithm for FM signals and, therefore, a good candidate for the DSI cancellation algorithm in the generalised processing chain.

7.1.2 LTE Signal Equalisation

To include LTE signals as part of the performance analysis of the processing chain, the ambiguities caused by signalling information needed to be removed. A thorough analysis of the LTE signal from the EAN network was performed to determine the Doppler and range ambiguities that are caused by the guard interval, the RS carriers and the SS carriers. The results of calculations, as presented in Table 5.3 when compared to AFs of a recorded LTE signal confirm the signalling information as the main cause of the ambiguities in LTE PR. Signal equalisation, so called in this dissertation, was used to suppress the signaling information to remove the ambiguities. This method is based on pilot suppression used for DVB-T2 signals. Using AFs of the LTE signal as well as ARD maps generated from LTE data with targets simulated in the data, it was demonstrated that by removing the guard interval from the signal and multiplying the RS and SS carriers with a factor of 0.007, the ambiguities can be removed and target detection becomes possible using ECA-CD and Batches.

7.1.3 Results

The proposed processing chain consists of ECA-CD DSI-cancellation and Batches ARD map generation. To determine the efficacy and efficiency of the proposed processing chain, targets were simulated in data of an FM signal, a DVB-T2 signal and an LTE signal and the resulting signals were processed using the proposed processing chain. The ARD maps produced showed satisfactory performance with the targets appearing at the expected range and doppler shifts. It was noted that the Batches approach creates an inverse relationship between the maximum bistatic range and the max/min Doppler shifts of the ARD map. This can be mitigated by increasing the CPI, however it was demonstrated, by comparing the DVB-T2 and LTE relative time results in Table 6.3, that this will increase the relative processing time creating another performance trade off to consider depending on the application of the PR. These results demonstrated that the proposed generalised processing chain works efficiently on both FM and OFDM signal structures. The goal of producing an efficient generalised processing chain

was realised using ECA-CD for DSI cancellation and Batches to produce the ARD map output.

7.2 Future Work

While the processing chain is efficient for processing both FM and OFDM siganls, it still requires significant optimisation to be real-time capable, especially in the case of processing the high bandwidth OFDM signals. Therefore, real-time optimisation would greatly enhance the efficiency of the processing chain and increase it's usability across more PR applications. To implement the processing chain into a real PR system, combining the ARD outputs of separate data processing streams, implementing a tracker and creating a visualisation in Cartesian coordinates are necessary additions to the processing chain. For a complete demonstration, the hardware for a combined PR system would need to be designed and assembled with the processing chain integrated and followed up with field tests using real-world targets such as aircraft at an airfield. The low computational load of the processing chain is promising for optimisation to create a real-time capable processing chain.

Bibliography

[1] S. Dhagle. [Online]. Available: http://dhagle.in/LTE

[2] "Ieee standard for radar definitions," *IEEE Std 686-2017 (Revision of IEEE Std 686-2008)*, pp. 1–54, 2017.

[3] S. T. Paine, "Electronic countermeasures applied to passive radar," Ph.D. dissertation, University of Cape Town, 2019.

[4] C. A. Tong, "A scalable real-time processing chain for radar exploiting illuminators of opportunity," Ph.D. dissertation, University of Cape Town, 2014.

[5] Y. Paichard and M. Inggs, "Multistatic passive coherent location radar systems," in *2009 European Radar Conference (EuRAD)*, 2009, pp. 45–48.

[6] D. O'Hagan, F. Colone, C. Baker, and H. Griffiths, "Passive bistatic radar (pbr) demonstrator," in *2007 IET International Conference on Radar Systems*, 2007, pp. 1–5.

[7] D. W. O'Hagan, "Passive bistatic radar performance characterisation using fm radio illuminators of opportunity," Ph.D. dissertation, University College London, 2009.

[8] B. Yildirim, "Passive radar: a potential solution for wlan sensing," https://www.abc.xyz/the_slides.pdf, 2019, accessed: 2022–11-12.

[9] C. Baker, H. Griffiths, and I. Papoutsis, "Passive coherent location radar systems. part 2: Waveform properties," *Radar, Sonar and Navigation, IEE Proceedings* -, vol. 152, pp. 160 – 168, 07 2005.

[10] C. Schüpbach, S. Paine, and D. O'Hagan, "Efficient direct signal cancellation for fm-based passive radar," in *2020 IEEE Radar Conference (RadarConf20)*, 2020, pp. 1–5.

[11] H. Griffiths and C. Baker, "The signal and interference environment in passive bistatic radar," in *2007 Information, Decision and Control*, 2007, pp. 1–10.

[12] B. A. Austin, "Precursors to radar — the watson-watt memorandum and the daventry experiment," *The International Journal of Electrical Engineering & Education*, vol. 36, no. 4, pp. 365–372, 1999. [Online]. Available: https://doi.org/10.7227/IJEEE.36.4.10

[13] H. Griffiths and N. Willis, "Klein heidelberg-the first modern bistatic radar system," *Aerospace and Electronic Systems, IEEE Transactions on*, vol. 46, pp. 1571 – 1588, 11 2010.

[14] H. Kuschel and D. O'Hagan, "Passive radar from history to future," in *11-th INTERNATIONAL RADAR SYMPOSIUM*, 2010, pp. 1–4.

[15] H. D. Griffiths and N. Long, "Television-based bistatic radar," 1986.

[16] D. W. O'Hagan and C. J. Baker, "Passive bistatic radar (pbr) using fm radio illuminators of opportunity," in *2008 New Trends for Environmental Monitoring Using Passive Systems*, 2008, pp. 1–6.

[17] H. Griffiths, A. Garnett, C. Baker, and S. Keaveney, "Bistatic radar using satellite-borne illuminators of opportunity," in *92 International Conference on Radar*, 1992, pp. 276–279.

[18] H. Griffiths, C. Baker, J. Baubert, N. Kitchen, and M. Treagust, "Bistatic radar using satellite-borne illuminators," in *RADAR 2002*, 2002, pp. 1–5.

[19] J. D. Sahr and F. D. Lind, "The manastash ridge radar: A passive bistatic radar for upper atmospheric radio science," *Radio Science*, vol. 32, no. 6, pp. 2345–2358, 1997.

[20] H. Griffiths and C. Baker, "Measurement and analysis of ambiguity functions of passive radar transmissions," in *IEEE International Radar Conference, 2005.*, 2005, pp. 321–325.

[21] ——, "Passive coherent location radar systems. part 1: Performance prediction," *Radar, Sonar and Navigation, IEE Proceedings* -, vol. 152, pp. 153 – 159, 07 2005.

[22] M. Inggs, C. Tong, D. O'Hagan, U. Bönigert, U. Siegenthaler, C. Schupbach, and H. Pratisto, "Noise jamming of a fm band commensal radar," in *2015 IEEE Radar Conference*, 2015, pp. 493–498.

[23] C. Tong and J. Coetser, "A minimal architecture for real-time, medium range aircraft detection using fm-band illuminators of opportunity," in *2015 IEEE Radar Conference (RadarCon)*, 2015, pp. 1250–1255.

[24] N. Morrison, R. Lord, and M. Inggs, "The gauss-newton algorithm applied to track-while-scan radar," in *2007 IET International Conference on Radar Systems*, 2007, pp. 1–5.

[25] ——, "The gauss-newton algorithm in passive aircraft tracking using doppler and bearings," in *2007 IET International Conference on Radar Systems*, 2007, pp. 1–5.

[26] R. Nadjiasngar, M. Inggs, Y. Paichard, and N. Morrison, "A new probabilistic data association filter based on composite expanding and fading memory polynomial filters," in *2011 IEEE RadarCon (RADAR)*, 2011, pp. 152–156.

[27] C. Tong, M. Inggs, and G. Lange, "Processing design of a networked passive coherent location system," in *2011 IEEE RadarCon (RADAR)*, 2011, pp. 692–697.

[28] C. Tong, M. Inggs, and A. Mishra, "Towards a mimo radar based on commensal use of fm broadcast transmitters of opportunity," in *EUSAR 2012; 9th European Conference on Synthetic Aperture Radar*, 2012, pp. 283–286.

[29] F. Maasdorp, R. Nadjiasngar, and M. Inggs, "A cramer rao analysis on receiver placement in a fm band commensal radar system based on doppler only measurements," in *2014 International Radar Conference*, 2014, pp. 1–6.

[30] M. Inggs, C. Tong, R. Nadjiasngar, G. Lange, A. Mishra, and F. Maasdorp, "Planning and design phases of a commensal radar system in the fm broadcast band," *IEEE Aerospace and Electronic Systems Magazine*, vol. 29, no. 7, pp. 50–63, 2014.

[31] P. Howland, D. Maksimiuk, and G. Reitsma, "Fm radio based bistatic radar," *Radar, Sonar and Navigation, IEE Proceedings* -, vol. 152, pp. 107 – 115, 07 2005.

[32] D. O'Hagan, H. Griffiths, S. Ummenhofer, and S. Paine, "Elevation pattern analysis of common passive bistatic radar illuminators of opportunity," *IEEE Transactions on Aerospace and Electronic Systems*, vol. PP, pp. 1–1, 07 2017.

[33] A. Schroeder and M. Edrich, "Cassidian multiband mobile passive radar system," in *2011 12th International Radar Symposium (IRS)*, 2011, pp. 286–291.

[34] C. Bongioanni, F. Colone, and P. Lombardo, "Performance analysis of a multi-frequency fm based passive bistatic radar," in *2008 IEEE Radar Conference*, 2008, pp. 1–6.

[35] M. Żywek and M. Malanowski, "Real-time selection of fm transmitter in passive bistatic radar based on short-term bandwidth analysis," in *2021 21st International Radar Symposium (IRS)*, 2021, pp. 1–10.

[36] DVB. (2022) Dtt deployment data. [Online]. Available: https://dvb.org/solutions/dtt-deployment-data/

[37] F. Colone, D. W. O'Hagan, P. Lombardo, and C. J. Baker, "A multistage processing algorithm for disturbance removal and target detection in passive bistatic radar," *IEEE Transactions on Aerospace and Electronic Systems*, vol. 45, no. 2, pp. 698–722, 2009.

[38] R. Saini and M. Cherniakov, "Dtv signal ambiguity function analysis for radar application," *Radar, Sonar and Navigation, IEE Proceedings* -, vol. 152, pp. 133 – 142, 07 2005.

[39] Z. Gao, R. Tao, Y. Ma, and T. Shao, "Dvb-t signal cross-ambiguity functions improvement for passive radar," in *2006 CIE International Conference on Radar*, 2006, pp. 1–4.

[40] C. R. Berger, B. Demissie, J. Heckenbach, P. Willett, and S. Zhou, "Signal processing for passive radar using ofdm waveforms," *IEEE Journal of Selected Topics in Signal Processing*, vol. 4, no. 1, pp. 226–238, 2010.

[41] H. A. Harms, L. M. Davis, and J. Palmer, "Understanding the signal structure in dvb-t signals for passive radar detection," in *2010 IEEE Radar Conference*, 2010, pp. 532–537.

[42] H. Kuschel, M. Ummenhofer, D. O'Hagan, and J. Heckenbach, "On the resolution performance of passive radar using dvb-t illuminations," in *11-th INTERNATIONAL RADAR SYMPOSIUM*, 2010, pp. 1–4.

[43] O. Mahfoudia, F. Horlin, and X. Neyt, "Optimum reference signal reconstruction for dvb-t based passive radars," in *2017 IEEE Radar Conference (RadarConf)*, 2017, pp. 1327–1331.

[44] J. E. Palmer, H. A. Harms, S. J. Searle, and L. Davis, "Dvb-t passive radar signal processing," *IEEE Transactions on Signal Processing*, vol. 61, no. 8, pp. 2116–2126, 2013.

[45] K. Pölönen and V. Koivunen, "Detection of dvb-t2 control symbols in passive radar systems," in *2012 IEEE 7th Sensor Array and Multichannel Signal Processing Workshop (SAM)*, 2012, pp. 309–312.

[46] D. A. Kovalev and V. I. Veremyev, "Correction of dvb-t2 signal cross-ambiguity function for passive radar," in *2014 International Radar Conference*, 2014, pp. 1–4.

[47] D. W. O'Hagan, M. Setsubi, and S. Paine, "Signal reconstruction of dvb-t2 signals in passive radar," in *2018 IEEE Radar Conference (RadarConf18)*, 2018, pp. 1111–1116.

[48] S. Paine, F. Schonken, M. Malape, D. W. O'Hagan, J. Swart, F. Louw, and M. Setsubi, "Multi band fm and dvb-t2 passive radar demonstrator," in *2018 19th International Radar Symposium (IRS)*, 2018, pp. 1–10.

[49] V. Winkler, C. Klöck, and M. Edrich, "Migration to the dvb-t2-standard for passive radar," in *2017 18th International Radar Symposium (IRS)*, 2017, pp. 1–10.

[50] E. Vorobev, A. Barkhatov, and V. Kutuzov, "Dvb-t2 passive coherent location radar," in *2016 IEEE NW Russia Young Researchers in Electrical and Electronic Engineering Conference (EICon-RusNW)*, 2016, pp. 470–474.

[51] E. Vorobev, A. Barkhatov, V. Veremyev, and V. Kutuzov, "Dvb-t2 passive radar developed at saint petersburg electrotechnical university," in *2018 22nd International Microwave and Radar Conference (MIKON)*, 2018, pp. 204–207.

[52] D. W. O'Hagan, H. Kuschel, J. Heckenbach, M. Ummenhofer, and J. Schell, "Signal reconstruction as an effective means of detecting targets in a dab-based pbr," in *11-th INTERNATIONAL RADAR SYMPOSIUM*, 2010, pp. 1–4.

[53] S. Searle, J. Palmer, L. Davis, D. W. O'Hagan, and M. Ummenhofer, "Evaluation of the ambiguity function for passive radar with ofdm transmissions," in *2014 IEEE Radar Conference*, 2014, pp. 1040–1045.

[54] D. Poullin, "Passive detection using digital broadcasters (dab, dvb) with cofdm modulation," *Radar, Sonar and Navigation, IEE Proceedings* -, vol. 152, pp. 143 – 152, 07 2005.

[55] "Standards - dvb-t2."

[56] S. Searle, S. Howard, and J. Palmer, "Remodulation of dvb—t signals for use in passive bistatic radar," in *2010 Conference Record of the Forty Fourth Asilomar Conference on Signals, Systems and Computers*, 2010, pp. 1112–1116.

[57] r. s. a. raja abdullah, F. Hashim, A. Salah, N. E. RASHID, A. Ismail, and H. Aziz, "Experimental investigation on target detection and tracking in passive radar using long-term evolution signal," *IET Radar, Sonar Navigation*, vol. 10, 09 2015.

[58] A. A. Salah, R. S. A. R. Abdullah, A. Ismail, F. Hashim, C. Y. Leow, M. B. Roslee, and N. E. A. Rashid, "Feasibility study of lte signal as a new illuminators of opportunity for passive radar

applications," in *2013 IEEE International RF and Microwave Conference (RFM)*, 2013, pp. 258–262.

[59] P. Rai, A. Kumar, M. Khan, and L. R. Cenkeramaddi, "Lte-based passive radars and applications: A review," *International Journal of Remote Sensing*, vol. 42, 08 2021.

[60] K. Li, C. Yuen, S. S. Kanhere, K. Hu, W. Zhang, F. Jiang, and X. Liu, "An experimental study for tracking crowd in smart cities," *IEEE Systems Journal*, vol. 13, no. 3, pp. 2966–2977, 2019.

[61] K. Chetty, G. E. Smith, and K. Woodbridge, "Through-the-wall sensing of personnel using passive bistatic wifi radar at standoff distances," *IEEE Transactions on Geoscience and Remote Sensing*, vol. 50, no. 4, pp. 1218–1226, 2012.

[62] A. Evers and J. A. Jackson, "Analysis of an lte waveform for radar applications," in *2014 IEEE Radar Conference*, 2014, pp. 0200–0205.

[63] ——, "Experimental passive sar imaging exploiting lte, dvb, and dab signals," in *2014 IEEE Radar Conference*, 2014, pp. 0680–0685.

[64] "Lte: Evolved universal terrestrial radio access (e-utra), physical channels and modulation," European Telecommunications Standards Institute, European Telecommunications Standards Institute, Tech. Rep., 2011, 2011. [Online]. Available: http://www.etsi.org/deliver/etsits/136200136299/136211/09.01.0060/ts136211v090100p.pdf.

[65] S. Sardar, A. K. Mishra, and M. Z. A. Khan, "Lte-commsense system and its feasibility analysis," in *2017 IEEE AFRICON*, 2017, pp. 1564–1568.

[66] R. Blázquez-García, J. Casamayón-Antón, and M. Burgos-García, "Lte-r based passive multistatic radar for high-speed railway network surveillance," in *2018 15th European Radar Conference (EuRAD)*, 2018, pp. 6–9.

[67] Z. Zhao, X. Wan, Q. hong Shao, Z. Gong, and F. Cheng, "Multipath clutter rejection for digital radio mondiale-based hf passive bistatic radar with ofdm waveform," *Iet Radar Sonar and Navigation*, vol. 6, pp. 867–872, 2012.

[68] C. Schwark and D. Cristallini, "Advanced multipath clutter cancellation in ofdm-based passive radar systems," in *2016 IEEE Radar Conference (RadarConf)*, 2016, pp. 1–4.

[69] D. Petri, C. Moscardini, M. Martorella, M. Conti, A. Capria, and F. Berizzi, "Performance analysis of the batches algorithm for range-doppler map formation in passive bistatic radar," in *IET International Conference on Radar Systems (Radar 2012)*, 2012, pp. 1–4.

[70] H. Kuschel, J. Heckenbach, D. O'Hagan, and M. Ummenhofer, "A hybrid multi-frequency passive radar concept for medium range air surveillance," in *2011 MICROWAVES, RADAR AND REMOTE SENSING SYMPOSIUM*, 2011, pp. 275–279.

[71] S. Paine, F. Schonken, M. Malape, D. W. O'Hagan, J. Swart, F. Louw, and M. Setsubi, "Multi band fm and dvb-t2 passive radar demonstrator," in *2018 19th International Radar Symposium (IRS)*, 2018, pp. 1–10.

[72] D. Petri, C. Moscardini, M. Martorella, M. Conti, A. Capria, and F. Berizzi, "Performance analysis of the batches algorithm for range-doppler map formation in passive bistatic radar," vol. 2012, 01 2012, pp. 1–4.

[73] F. G. Stremler, *Introduction to communication systems, third edition.* Pearson, 1990.

[74] M. Brooker, "The design and implementation of a simulator for multistatic radar systems," Ph.D. dissertation, University of Cape Town, 2008.

[75] RRSG. (2022) Fers wiki. [Online]. Available: https://github.com/stpaine/FERS/wiki

[76] R. Prasad, *OFDM for Wireless Communications Systems*, 2004.

[77] "Etsi ts 136 211 v15.13.0 (2021-05) lte; evolved universal terrestrial radio access (e-utra); physical channels and modulation (3gpp ts 36.211 version 15.13.0 release 15)," ETSI T, France, RF, Standard, May 2021.

[78] S. Paine, S. Schonken, D. O'Hagan, and C. Schupbach, "Comparison of different range-doppler processing techniques for ofdm based dvb-t2 passive radar," *UNPUBLISHED.*

[79] L. Zawadka and L. Maślikowski, "Dvb-t based passive radar demonstrator using digital correlator implemented on ni flexrio platform," in *2013 Signal Processing Symposium (SPS)*, 2013, pp. 1–4.

[80] A. Capria, D. Petri, M. Martorella, M. Conti, E. Dalle Mese, and F. Berizzi, "Dvb-t passive radar for vehicles detection in urban environment," in *2010 IEEE International Geoscience and Remote Sensing Symposium*, 2010, pp. 3917–3920.

[81] M. T. Malape, "Implementation of a dvb-t2 passive coherent locator demonstrator," Master's thesis, University of Cape Town, 2019.

Appendix A

Proof of OFDM Carrier Orthogonality

Statement: Given two complex exponential signals with frequencies that differ by $\Delta\omega = \frac{2\pi k}{T_u}$, the signals are orthogonal over an integration period of T_u for any integer value of k.

Proof: Consider the two complex exponential signals that differ by a frequency of $\Delta\omega$,

$$\psi_1 = \rho_1 \cdot e^{j(\omega_0 t + \theta_1)} \tag{A.1}$$

$$\psi_2 = \rho_2 \cdot e^{j((\omega_0 + \Delta\omega)t + \theta_2)} \tag{A.2}$$

where ρ_1 and ρ_2 are arbitrary real values, and θ_1 and θ_2 are arbitrary phase-shifts.

The inner product of the two signals over an integration period of T_u is defined as,

$$\langle \psi_1, \psi_2 \rangle := \int_0^{T_u} \psi_1(t)\psi_2^*(t)\, dt \tag{A.3}$$

where $\psi_2^*(t)$ is the complex conjugate of $\psi_2(t)$. Substituting ψ_1 and ψ_2, and then simplifying,

$$\langle \psi_1, \psi_2 \rangle = \int_0^{T_u} \rho_1 e^{j(\omega_0 t + \theta_1)} \cdot \rho_2 e^{-j((\omega_0 + \Delta\omega)t + \theta_2)}\, dt \tag{A.4}$$

$$= \rho_1\rho_2 \int_0^{T_u} e^{j(\omega_0 t + \theta_1 - \omega_0 t - \Delta\omega t - \theta_2)}\, dt \tag{A.5}$$

$$= \rho_1\rho_2 e^{j(\theta_1 - \theta_2)} \int_0^{T_u} e^{-j\Delta\omega t}\, dt \tag{A.6}$$

Letting $C = \rho_1\rho_2 e^{j(\theta_1 - \theta_2)}$, substituting $\Delta\omega = \frac{2\pi k}{T_u}$, and calculating the definite integral,

$$\langle \psi_1, \psi_2 \rangle = C \cdot \frac{1}{-j2\pi\frac{k}{T_u}} \left[e^{-j2\pi\frac{k}{T_u}t} \right]_{t=0}^{t=T_u} \tag{A.7}$$

$$= C \cdot \frac{1}{-j2\pi\frac{k}{T_u}} (e^{-j2\pi k} - 1) \tag{A.8}$$

Since $e^{-j2\pi k} = 1 \,\forall\, k \in \mathbb{Z}$,

$$\langle \psi_1, \psi_2 \rangle = 0 \tag{A.9}$$

Therefore, ψ_1 and ψ_2 are orthogonal over the integration period T_u.